Human TrkA^R649W mutation impairs nociception, sweating and cognitive abilities: a mouse model of HSAN IV

Paola Pacifico[1,†], Giovanna Testa[1,†], Rosy Amodeo[2,3], Marco Mainardi[1,4], Alexia Tiberi[1], Domenica Convertino[2,3],

Juan Carlos Arevalo[5,6], Laura Marchetti[2,7], Mario Costa[4,8], Antonino Cattaneo[1,9,‡,*] and Simona Capsoni (iD)[1,10,‡,*]

[1]Bio@SNS Laboratory, Scuola Normale Superiore, Pisa 56124, Italy
[2]Center for Nanotechnology Innovation @NEST, Istituto Italiano di Tecnologia, Pisa 56127, Italy
[3]NEST, Scuola Normale Superiore, Pisa 56127, Italy
[4]Neuroscience Institute, National Research Council (IN-CNR), Pisa 56124, Italy
[5]Departmento de Biología Celular y Patología, Instituto de Neurociencias de Castilla y León, University of Salamanca, Salamanca 37007, Spain
[6]Institute of Biomedical Research of Salamanca, Salamanca 37007, Spain
[7]Department of Pharmacy, University of Pisa, Pisa 56126, Italy
[8]Pisa Center for Research and Clinical Implementation Flash Radiotherapy (CPFR@CISUP), Pisa 56126, Italy
[9]Rita Levi-Montalcini European Brain Research Institute (EBRI), Rome 00161, Italy
[10]Department of Neuroscience and Rehabilitation, Institute of Physiology, University of Ferrara, Ferrara 44121, Italy

*To whom correspondence should be addressed. Email: antonino.cattaneo@sns.it and simona.capsoni@sns.it
†Co-first authorship
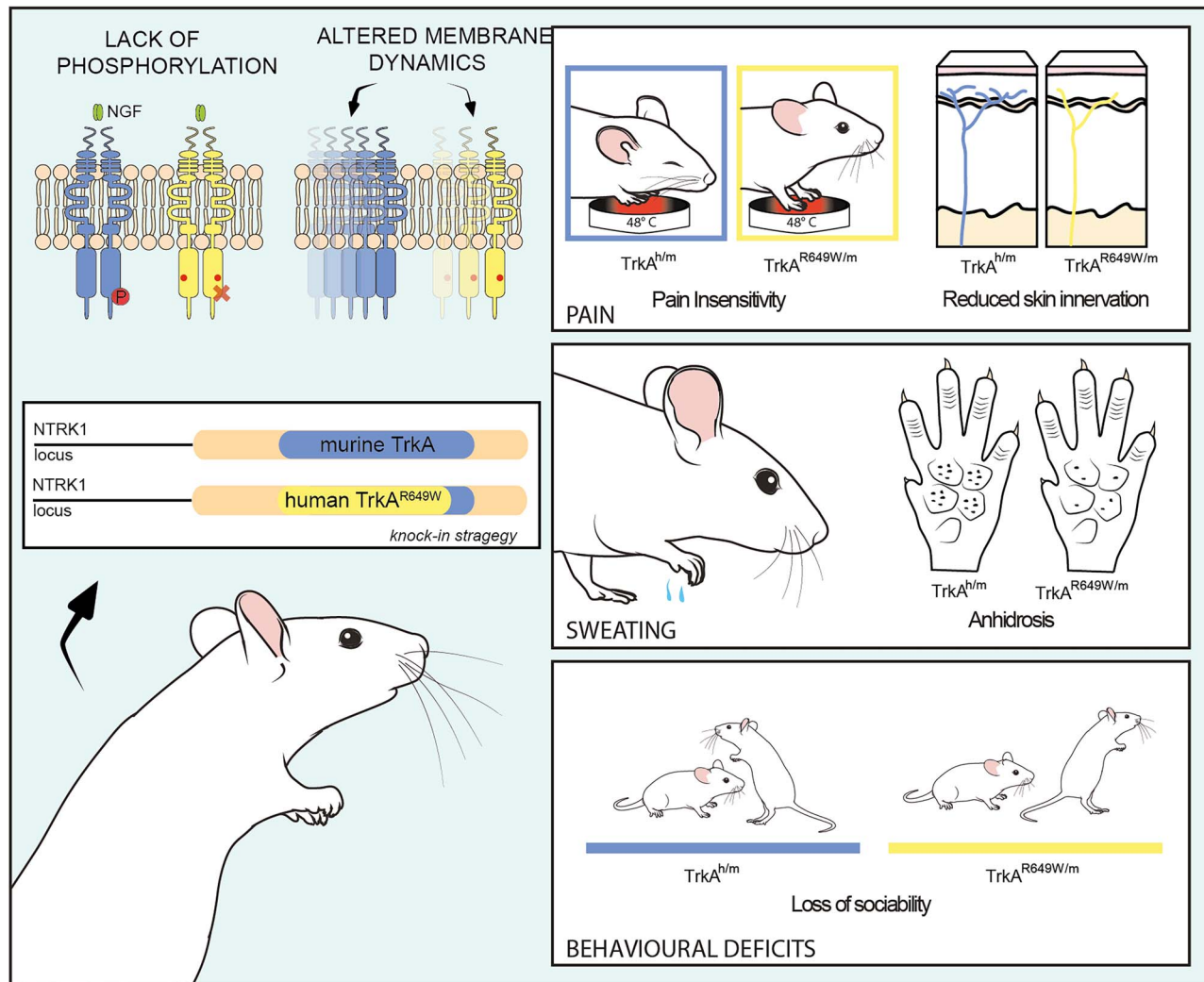‡Joint corresponding authors

Abstract

A functional nerve growth factor NGF–Tropomyosin Receptor kinase A (TrkA) system is an essential requisite for the generation and maintenance of long-lasting thermal and mechanical hyperalgesia in adult mammals. Indeed, mutations in the gene encoding for TrkA are responsible for a rare condition, named Hereditary Sensory and Autonomic Neuropathy type IV (HSAN IV), characterized by the loss of response to noxious stimuli, anhidrosis and cognitive impairment. However, to date, there is no available mouse model to properly understand how the NGF–TrkA system can lead to pathological phenotypes that are distinctive of HSAN IV. Here, we report the generation of a knock-in mouse line carrying the HSAN IV TrkA^R649W mutation. First, by *in vitro* biochemical and biophysical analyses, we show that the pathological R649W mutation leads to kinase-inactive TrkA also affecting its membrane dynamics and trafficking. In agreement with the HSAN IV human phenotype, TrkA^R649W/m mice display a lower response to thermal and chemical noxious stimuli, correlating with reduced skin innervation, in addition to decreased sweating in comparison to TrkA^h/m controls. Moreover, the R649W mutation decreases anxiety-like behavior and compromises cognitive abilities, by impairing spatial-working and social memory. Our results further uncover unexplored roles of TrkA in thermoregulation and sociability. In addition to accurately recapitulating the clinical manifestations of HSAN IV patients, our findings contribute to clarifying the involvement of the NGF–TrkA system in pain sensation.

Graphical Abstract

Introduction

Pain perception is a warning system that has evolved to preserve the physical integrity of the body and diminish tissue and cellular damage, with the ultimate goal of enhancing survival. After injury, a wide range of chemical mediators are released (1). Among them, nerve growth factor (NGF) (2) is a member of the neurotrophin family (3) known for its actions on the differentiation and survival of target neurons in both the central and peripheral nervous systems (4). NGF actions are mediated via the tyrosine kinase TrkA (5,6) and p75[NTR] receptors (7,8,9) in neuronal and non-neuronal cells (10–13). In adults, the primary function of NGF in the periphery is to mediate neuronal sensitization and inflammatory responses after tissue damage (14–16). Injection of NGF produces extensive and long-lasting thermal and mechanical hyperalgesia both in laboratory animals and in humans (17–19), while the infusion of neutralizing antibodies against NGF or TrkA reduces behavioral responses to noxious stimuli in animals (20–22) and has an analgesic effect in human patients suffering from chronic and inflammatory pain conditions (23,24).

The crucial role of the NGF–TrkA signaling axis in pain transmission is evident in two rare congenital pain insensitivity diseases: the Hereditary Sensory and Autonomic Neuropathy

(HSAN) types IV and V, linked to mutations in the *NTRK1* and *NGF* genes, respectively (25,26). The *NTRK1 (TRKA)* mutations with the highest phenotypic effects map within the intracellular tyrosine kinase domain (TKD), whereas the few mutations involving residues in the extracellular domain lead to a milder clinical manifestation (27–30). Both *NTRK1* and *NGF* mutations similarly provoke the inability to perceive painful stimuli, leading to injuries, self-mutilations and infections (25,31–35). On the other hand, distinctive traits of HSAN IV are represented by anhidrosis, which predisposes to recurrent episodes of fever, and by variable degrees of mental retardation (36), which are not found in homozygous HSAN V patients (34,37,38). Here, we now describe the generation and characterization of HSAN IV *NTRK1* knock-in mice, harboring the *NTRK1* missense R649W mutation and show that, similarly to human disease, this model reproduces anhidrosis, reduced anxiety, and impaired spatial-working and social memory. Thus, by characterizing the phenotype of HSAN IV knock-in mice, and comparing it to an animal model reproducing a related 'painlessness' disease, we contribute to clarifying the role of the NGF–TrkA signaling system in pain transmission and sensation and provide new insights into the pathogenesis of these conditions.

Results

Choice of HSAN IV mutation

HSAN IV is a rare autosomal recessive disorder linked to mutations in *NTRK1*. Genetic analyses of HSAN IV patients have identified more than 100 mutations in *NTRK1* (HGMD 2021.4). Mutations are distributed all along the protein sequence of TrkA, from the extracellular to the kinase domain, but most of them are missense and non-sense mutations in the cytoplasmic domain of the receptor. Missense mutations affecting the kinase domain disturb the ligand-induced kinase activity of TrkA. The functional analysis of a group of missense mutations in TKD, including Arg649Trp (R649W), shows a diminished kinase activity and reduced autophosphorylation after NGF stimulation in transfected cells (28–30), and this manuscript). The importance of the Arg in 649 positions (R649-) has also been observed by Altassan and colleagues (39), investigating HSAN IV patient carrying the TrkA R649Q mutation. The Arg649- substitution seems to alter the residue charge affecting the stability of TrkA receptor during NGF-binding and leading to altered phosphorylation. The neighbor mutations L694P and G571R cause a similar R649W phenotype leading to pain and temperature insensitivity, anhidrosis and speech delay in patients pointing out the robust link between TKD TrkAmutations and HSAN IV disease (36,39,40). Indeed, structural mapping of HSAN IV TrkA variants has recently indicated that mutations located in TKD can affect the TrkA interaction with substrates, such as PLCγ, and these damages in TrkA-PLCγ interactions may have an analgesic effect on pain states in mice (41), given that the recruitment of PLCγ to TrkA is essential for NGF-mediated sensitization (42). In addition to mutations in the TKD mutations, other HSAN IV TrkA mutations are located in the extracellular domain, such as L213P. This class of mutations causes TrkA retention in the ER, impairing the export of TrkA to the membrane and its trafficking (27,29,30). There are, as well, nucleotide deletions that cause a frameshift introducing a premature stop codon, as with the Gly181fsX58 mutation located in the extracellular domain that results in a truncated TrkA impairing the NGF–TrkA binding (43). Finally, other mutations such as the supposed HSAN IV-linked C752S mutation do not affect the TrkA autophosphorylation and trafficking, nor neurite outgrowth in cell assays (44). Since the diversity of these HSAN IV mutations determines variable degrees of clinical phenotype and intellectual disabilities in affected individuals, we have decided to investigate in depth the missense Arg649Trp (R649W) mutation, located in TrkA TKD (Fig. 1A), first identified in a Spanish family (28), with the ultimate goal to shed light on the contribution of TrkA TKD mutations to HSAN IV disease.

After a biochemical and biophysical characterization of the mutant TrkA receptor, we generated the HSAN IV TrkA$^{R649W/m}$ knock-in mouse line and, as the control group, we used the heterozygous (AMB1-TrkA/170608) TrkA$^{h/m}$ mice, which represent the most proper control as they underwent the same knock-in strategy as TrkA$^{R649W/m}$ mice, to achieve the expression of the wild type human NTRK1 in the corresponding mouse locus.

The TrkA^{R649W} mutant receptor shows reduced NGF-induced phosphorylation and altered membrane dynamics in transfected cells

We first aimed to analyze whether the R649W mutation may affect the response of TrkA to the neurotrophin NGF. In line with previous findings (27–30), we found that NGF binding to human TrkA^{R649W} mutant receptors, expressed by transfection in HEK293 cells, resulted in a greatly reduced phosphorylation in comparison to TrkA^{WT}, whereas the total amount of protein was not altered (Fig. 1B).

In addition, we tested TrkA ubiquitination (45,46), a physiologically important mechanism regulating TrkA function *in vivo*, also in nociceptive neurons (47,48). We found that the R649W mutation resulted in a pronounced reduction of constitutive ubiquitination in HEK293 cells, compared to control TrkA^{WT} (Fig. 1C).

Given that NGF-induced membrane mobility and tyrosine kinase activity of TrkA are correlated (49), the mobility of the TrkA^{R649W} receptor on the membrane of living cells was investigated by single-particle tracking (SPT) and total internal reflection fluorescence (TIRF) microscopy (50). This method relies on the site-directed stoichiometric labeling of the TrkA with brilliant organic dyes or quantum dots via the S6 chemical tag inserted at its N-terminus (51). The S6-tagged TrkA receptor remains fully functional (49,50). The mutant TrkA^{R649W} receptor was therefore tagged with the S6 tag and labeled, in order to visualize and record its activity. To do so, we performed SPT measurements of TrkA^{WT} and TrkA^{R649W} membrane diffusion in living human neuroblastoma SK-N-BE cells, in order to investigate if and how the R649W mutation influences the receptor dynamics. Quantitative analysis of the diffusion coefficient (D) confirmed the typical bimodal distribution of D values of TrkA^{WT} trajectories, and the inversion of the relative population of the fast and slow D peaks induced by NGF stimulation (49,50). Conversely, TrkA^{R649W} trajectories appeared to diffuse almost four times more slowly than TrkA^{WT} ones, both in the absence and in the presence of NGF (Fig. 2A). This result was further supported by the analysis of the 2D distribution of D and γ coefficients, calculated using the MSS-TAD algorithm (50,52). This analysis showed that the trajectories of single TrkA^{R649W} receptors were not modulated by NGF stimulation, as opposed to the strong modulation of single-particle membrane dynamics induced by NGF in wild-type TrkA receptors (Fig. 2B). This shows that the main determinant of the membrane dynamics of TrkA receptors is not the NGF binding event, but its NGF-induced phosphorylation.

We then analyzed by TIRF microscopy the membrane pools of TrkA^{WT} and TrkA^{R649W} receptors, labeled with Qdots. Quantification of the density of labeled receptors per cell area (n. spots/μm^2) highlighted an increased membrane pool in cells expressing TrkA^{R649W} compared to wild-type human TrkA (Fig. 2C), despite the total amount of TrkA protein being the same, as shown in Figure 1B and in Supplementary Material, Figure S3.

The kinetics of NGF-induced internalization of TrkA^{WT} and TrkA^{R649W} receptors, was investigated in SK-N-BE cells by quantifying the density of Qdot-labeled receptors exposed on the cell membrane at different times after NGF addition (Fig. 2D). The normalized densities of Qdot-labeled spots were almost superimposable for TrkA^{WT} and TrkA^{R649W} receptors, at all time points analyzed, showing that the kinetics of NGF-induced internalization of TrkA^{WT} and TrkA^{R649W} receptors are the same (Fig. 2D). In order to have a more comprehensive view of the membrane trafficking of the two TrkA receptors, these were transfected in primary dorsal root ganglia (DRG) neurons. S6-tagged TrkA^{WT} and TrkA^{R649W} were labeled with Qdots, while immunofluorescence using a-TrkA antibody was used to mark the whole receptor pool. Importantly, S6 labeling was performed either in resting conditions or after a 1-h incubation of the neurons with 125 ng/ml NGF. This time window allows us to appreciate both ligand-induced TrkA internalization and recycling back to the membrane (53). Quantification of the Qdot/TrkA ratio in DRG neurons showed that the TrkA^{R649W} membrane pool, normalized to the total amount of receptor, is increased with respect to that of TrkA^{WT} (Fig. 2E)
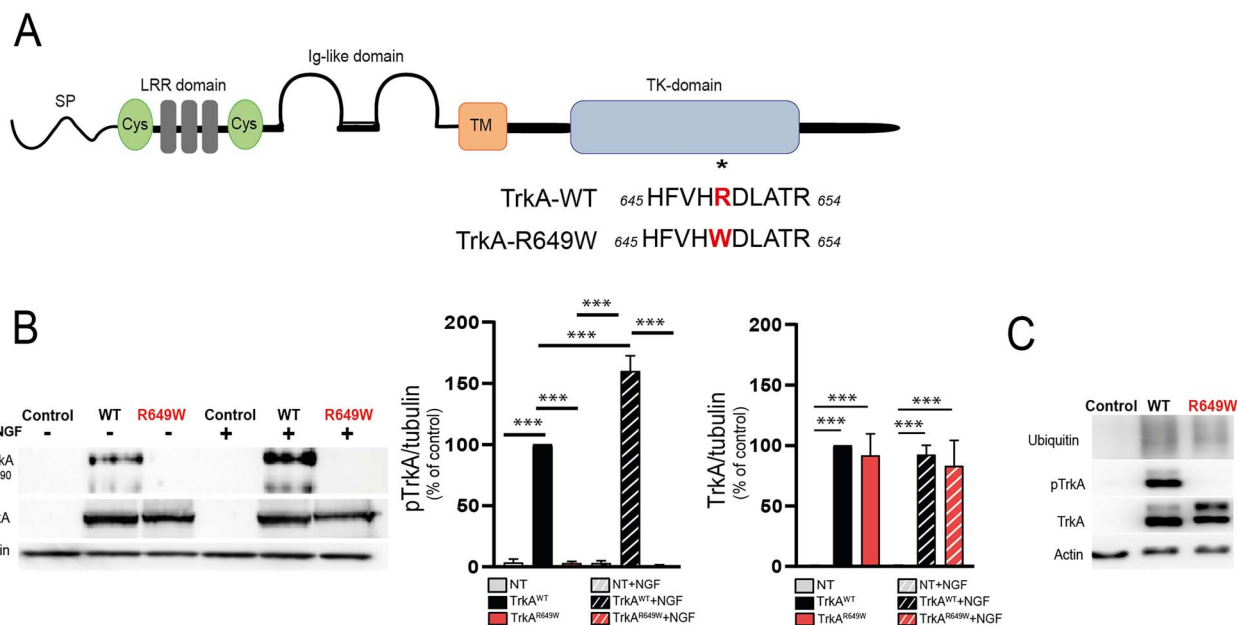
Figure 1. The R649W mutation affects TrkA phosphorylation and ubiquitination. (**A**) Schematic cartoon of TrkA domains. The asterisk shows the position of the R649W mutation. Bottom: Amino acid sequence alignment of the TKD of human TrkA. The mutated residue is indicated in red. (SP: signal peptide. Cys: cysteine-rich domains. LRR: Leucine-rich region. Ig: immunoglobulin-like domain. TM: transmembrane domain. TKD: tyrosine kinase domain). (**B**) Representative WB and quantification showing TrkA phosphorylation and total TrkA levels in Hek293 cells transfected with human TrkA^{WT} and human TrkA^{R649W}, in the presence (+) or absence (−) of stimulation with 100 ng/ml of NGF for 30 min. Tubulin was used as a loading control in WB. The mutation severely affects the response of mutant TrkA to NGF stimulation. Two-way ANOVA $F_{(2,12)} = 22.264$, $P \leq 0.001$ followed by Bonferroni post-hoc test (***$P \leq 0.001$); TrkA: Two-way ANOVA $F_{(2,9)} = 0.226$, $P \leq 0.001$ followed by Bonferroni post-hoc test (***$P \leq 0.001$). (**C**) Representative WB with anti-ubiquitin antibodies showing that constitutive ubiquitination of TrkA^{R649W} is significantly reduced with respect to TrkA^{WT}.

also in DRG neurons. However, upon NGF stimulation for 1 h, the increased membrane pool of TrkA^{R649W} was drastically reduced, with respect to the membrane pool of TrkA^{WT}, which remained constant (Fig. 2E). This effect was even stronger when the same quantification was selectively performed at the level of the growth cones, accounting for a ~72% average reduction of TrkA^{R649W} membrane pool, while no effect is observed in cells expressing TrkA^{WT} (Fig. 2F). Taken together, the data obtained in SK-N-BE and DRG cells show that the mutant TrkA^{R649W} displays a higher membrane abundance than TrkA^{WT}, which can be a consequence of alterations in recycling due to the reduced basal ubiquitination. Altogether, these profound alterations deserved a detailed investigation of the *in vivo* consequences of TrkA^{R649W} mutation, prompting us to develop a genetic mouse model of the HSAN IV disease.

Generation of TrkA^{R649W} knock-in mice: early postnatal lethality of homozygous mice

In order to generate a knock-in mouse line for HSAN IV carrying the R649W mutation in the human *NTRK1* (*TRKA*) gene, we adopted a targeted gene approach based on the in-frame replacement of the exon 1 coding sequence, as well as of part of intron 1, of the murine NTRK1 gene with the complete coding sequence of the human ortholog *NTRK1* gene, yielding the humanized wild-type TrkA knock-in mouse line (AMB1-TrkA/170608). To generate the human TrkA^{R649W} knock-in mouse line, the starting point was the targeting vector AMB1-Tg-pA, containing the coding sequence of the human NTRK1 (*TRKA*), which was used to generate the humanized TrkA knock-in mouse line (AMB1-TrkA/170608, or TrkA$^{h/m}$ mice). We used the targeting vector AMB1-Tg-pA, containing the human *NTRK1* cDNA coding sequence, to introduce the HSAN IV R649W mutation in human *NTRK1* cDNA by site-specific mutagenesis PCR. As shown in Figure 3A, the *NTRK1* cDNA

cassette, followed at the 3′ end by an exogenous hGH polyA cassette and a loxP-neomycin-loxP cassette, replaced the exon 1 as well as part of intron 1 of the murine Ntrk1 gene. The resulting mouse line was mated with 'Cre-deleter' mice to remove the neomycin selection cassette (Fig. 3A), thus generating heterozygous mice carrying the human mutant TrkA^{R649W} allele (TrkA$^{R649W/m}$ mice).

Homozygous mice (TrkA$^{R649W/R649W}$) were obtained by cross-breeding heterozygous mice (TrkA$^{R649W/m}$ mice) carrying one human TrkA^{R649W} allele and one murine allele. While heterozygous mice thrive to adulthood, TrkA$^{R649W/R649W}$ mice die within the first week of life. Representative pictures of pups at P0 show that at birth TrkA$^{R649W/R649W}$ pups were normal and the body size was comparable to that of heterozygous littermates, whereas at P4 the body size of TrkA$^{R649W/R649W}$ mice was lower than controls (Fig. 3C).

The homozygous condition of TrkA$^{R649W/R649W}$ mice matches the lethality observed in fully TrkA-deficient (TrkA$^{-/-}$) mice (54). This suggests that the loss of productive NGF–TrkA signaling in TrkA-expressing cells is a main consequence of the R649W mutation, in line with the experiments in cultured cells (Fig. 1).

Defective responses to pain and mechanical stimuli in TrkA$^{R649W/m}$ mice

Since homozygous TrkA$^{R649W/R649W}$ mice do not thrive to adulthood, we analyzed the phenotypic consequences of the R649W mutation in heterozygous TrkA$^{R649W/m}$ mice, in comparison to the control line TrkA$^{h/m}$ mice. Since these mice have never been phenotypically characterized, before comparing them to TrkA$^{R649W/m}$ we verified whether they behave similarly to wild-type mice (TrkA$^{m/m}$). As shown in Supplementary Material, Figure S1, the response to noxious thermal stimuli (acetone drop and Hot plate), and cognitive abilities (Y-maze and elevated plus maze) of TrkA$^{h/m}$
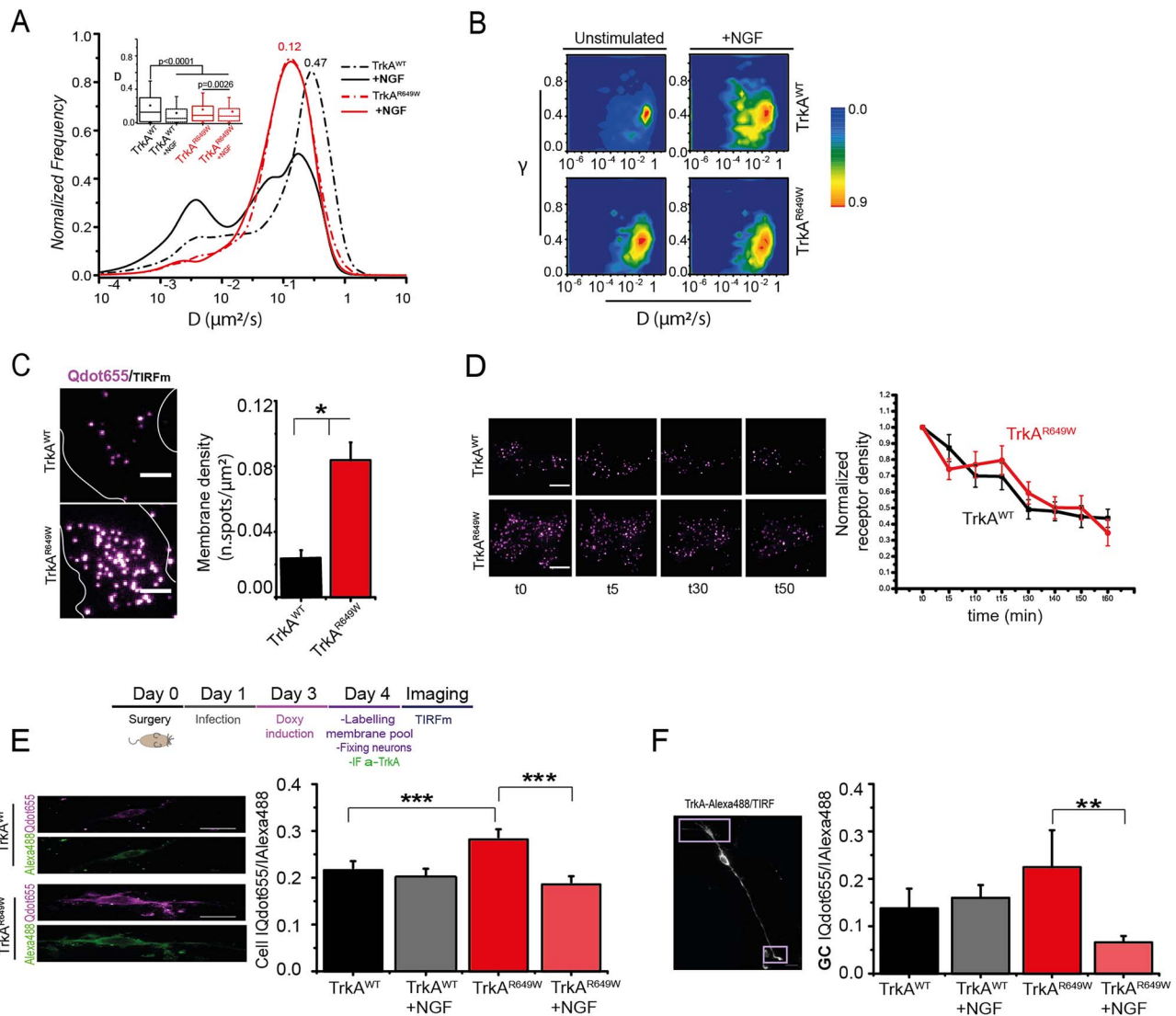
Figure 2. Effect of R649W mutation on TrkA membrane dynamics: biophysical studies. (A) SPT of TrkA[WT] and TrkA[R649W] receptors on the membrane of living human neuroblastoma SK-N-BE cells, viewed by TIRF microscopy. Distribution of diffusion coefficient (D) obtained from TrkA[WT] trajectories before (black solid curve, $n = 3369$ trajectories from 25 cells) and after NGF administration (125 ng/ml for 15 min) (black dotted curve, $n = 3283$ trajectories from 28 cells) and for TrkA[R649W] trajectories before (red solid curve, $n = 3638$ trajectories from 31 cells) and after NGF administration (red dotted curve, $n = 3375$ trajectories from 27 cells). On the left: box-plot for D values retrieved from the same trajectories (at least six frames long) of TrkA[WT] before (black solid) and after NGF administration (black dotted) and for TrkA[R649W] before (red solid) and after NGF administration (red dotted). Trajectories are pooled from two independent measures. Boxes: 25th–75th percentiles; whiskers: 10th–90th percentile; line: median; square: mean. $P < 0.0001$ and $P = 0.0026$ according to Kruskal-Wallis test, with Dunn's means comparison. **(B)** Total D-γ distributions according to MSS-TAD analysis of the same trajectories reported in A, for TrkA[WT] and TrkA[R649W] before and after NGF administration. On the right, logarithmic-scale color code for the frequency of the total D-γ distributions, normalized to 1 at the peak. **(C)** TIRF images of Qdot-labeled single receptor molecules of TrkA[WT] (upper) and TrkA[R649W] (lower); scale bar = 10 μm. On the right: quantification of density of labeled receptors per cell area (n.spots/μm^2) in SHSY5Y cells, obtained from three experimental replicates ($n = 22$ cells for TrkA[WT] $n = 12$ cells for TrkA[R649W]). *$P < 0.05$ according to two-tailed Mann–Whitney test. **(D)** Left: Representative TIRF images of single receptor spots of TrkA[WT] (top) and TrkA[R649W] (bottom) during a time-course after NGF stimulation. Every image corresponds to a time point of the same cell: t0 (time of NGF administration), t5, t30, t50 min. Scale bar = 10 μm. Right: Normalized membrane density for TrkA[WT] (black) and rTrkA[R649W] (red) is reported as mean ± SEM from cells acquired at each time point normalized for the respective density at time 0. $P_{construct} > 0.05$, $P_{time} < 0.001$, and $P_{constructxtime} > 0.05$ according to a two-way ANOVA test. All data are pools from 36 (TrkA[WT]) and 59 (TrkA[R649W]) cells, collected in two independent replicas. **(E)** Schematic timeline of the experimental procedure for the detection of the TrkA membrane pool in DRG neurons. Left: TIRF images of Qdot-labeled membrane TrkA[WT] and TrkA[R649W] receptors (magenta) and corresponding immunostained DRG neurons (green) infected with lentiviral particles bearing S6-tagged TrkA[WT] and TrkA[R649W] transgenes. Scale bar: 20 m. Right: Quantification of the membrane pool fraction on the total pool of TrkA[WT] and TrkA[R649W] in DRG neurons before and after 1 h of NGF stimulation (125 ng/ml). Quantification is obtained from the ratio between the intensity of Qdot signal (membrane receptors) against the intensity of Alexa488 (TrkA immunostaining) measured in the whole neuron (TrkA[WT] $n = 102$ neurons; TrkA[WT] + NGF $n = 21$ neurons; TrkA[R649W] $n = 87$ neurons, TrkA[R649W] + NGF $n = 43$ neurons). ***$P < 0.001$ according to Kruskal-Wallis Test. **(F)** Left: representative TIRF image of DRG neuron immunostained against TrkA with secondary antibody conjugated with Alexa488; growth cones are within the light purple boxes; scale bar: 20 nm. Right: quantification of TrkA membrane pool at growth cones before (TrkA[WT] $n = 17$ neurons and TrkA[R649W] $m = 11$ neurons) and after 1 h of NGF stimulation (125 ng/ml) (TrkA[WT] $n = 10$ neurons and TrkA[R649W] $n = 10$ neurons); **$P < 0.01$ according to Kruskal-Wallis test.
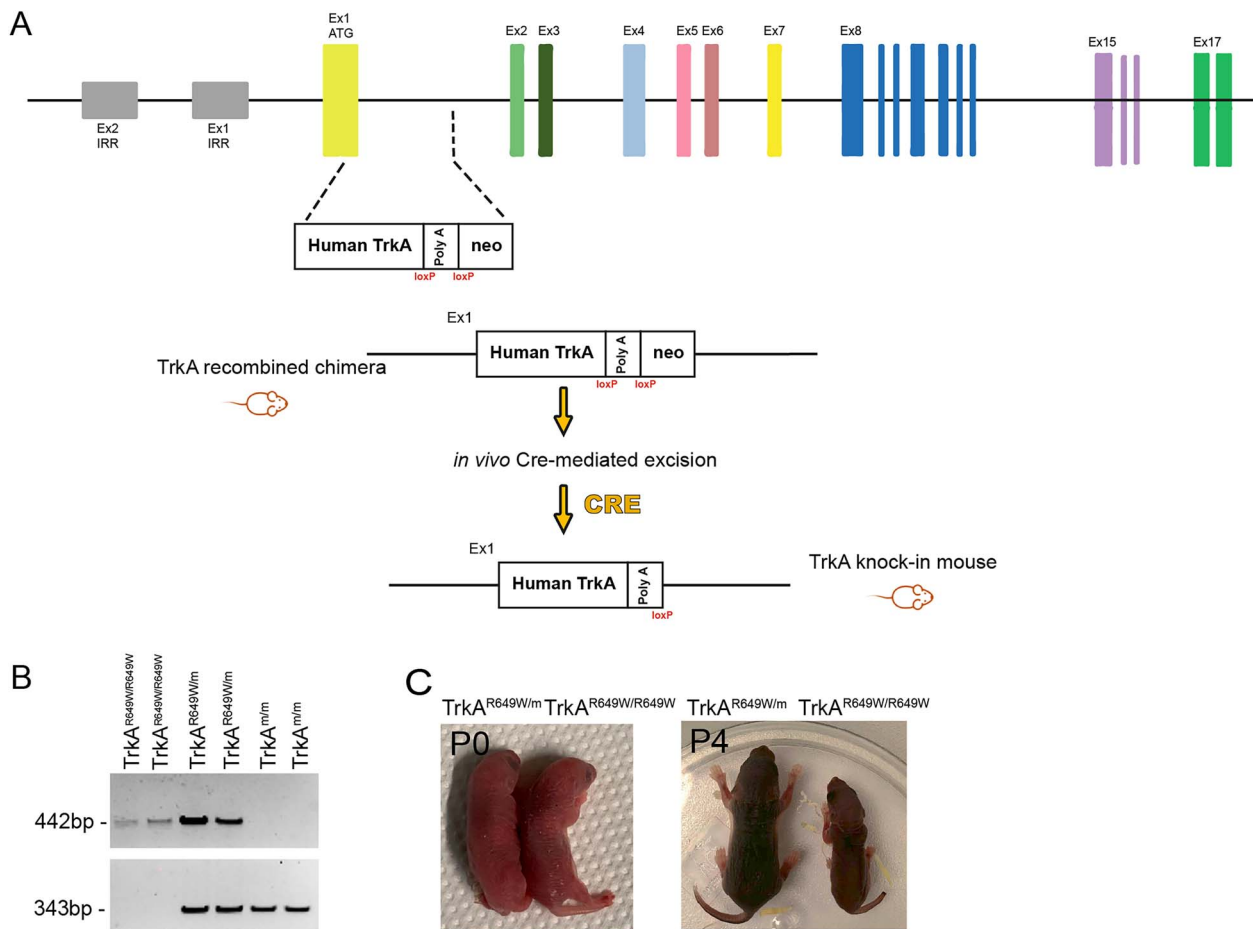
Figure 3. Generation of human TrkA[R649W] knock-in mice. (**A**) Molecular strategy to generate the human TrkA[R649W] knock-in mouse. Diagram illustrating the gene-targeting strategy to produce the TrkA[R649W] knock-in mice. Human TrkA cDNA cassette harboring the missense C-to-T mutation at the 1945 position replaced the murine TrkA exon 1 locus (corresponding to the R649W amino acid substitution). (**B**) PCR genotyping of homozygous (TrkA[R649W/R649W]), heterozygous (TrkA[R649W/m]) and wild-type (TrkA[m/m]) mice; wild-type band: 343 bp, mutant band: 442 bp. (**C**) Representative pictures of TrkA[R649W] knock-in mice. Homozygous mice appeared normal at birth (P0), but failed to grow during early postnatal life (e.g. at P4) compared to TrkA[R649W/m].

mice and wild-type mice (TrkA[m/m]) were similar, as well as the expression of DRGs markers.

One of the most characteristic and salient manifestations of HSAN IV is a generalized insensitivity to pain and thermal stimuli (35,55). To elucidate the consequences of the R649W mutation in peripheral somatosensation, we analyzed the phenotype of heterozygous TrkA[R649W/m] at 2 months of age. We performed an array of behavioral tests to evaluate the sensory responses to thermal, chemical and mechanical stimuli. We first tested the response to cold noxious stimuli induced by acetone application on the hindpaw. A significant decrease was observed both in the score and in the percentage of responses (Fig. 4A and B). The response threshold to a noxious high-temperature stimulus, was also significantly reduced in TrkA[R649W/m] compared to the control group (Fig. 4C). To test if the altered thermal sensation was specifically due to the R649W mutation or to functional haploinsufficiency, we compared TrkA[R649W/m] mice with heterozygous knock-out mice lacking one TrkA allele (TrkA^{+/−}). Strikingly, TrkA^{+/−} mice showed comparable behavioral responses to that of wild-type TrkA^{+/+} mice (Fig. 4D–F).

Moreover, intraepidermal injection of capsaicin, which evokes a prolonged pain sensation in TrkA[h/m] mice, via activation of TRPV1 receptors (56), failed to do so in TrkA[R649W/m] mice (Fig. 4G).

To test the response to innocuous mechanical stimuli, we used the tape response assay (57) and the von Frey test. We found a decrease in the number of attempts to remove the adhesive tape attached to the back of TrkA[R649W/m] mice, compared to TrkA[h/m] (Fig. 4H). On the other hand, no differences in the response to mechanical stimuli applied on the plantar surface of the hindpaw were observed between TrkA[R649W/m] and TrkA[h/m] mice (Fig. 4I). The different effect of the R649W mutation on mechanosensation is possibly due to distinct functional and anatomical properties of hairy and glabrous skin (58) and to deficits in the growth of hair follicles (59). These behavioral data indicate that TrkA[R649W/m] mice, unlike heterozygous TrkA^{+/−} mice, show a significant inability to sense thermal and chemical noxious stimuli and to respond to innocuous touch. This suggests a mutation-specific effect, distinct from a simple effect of wild-type TrkA haploinsufficiency.

Alteration of neuronal subpopulations in dorsal root ganglia from TrkA[R649W/m] mice

In order to obtain a phenotypic portrait of DRGs in the TrkA[R649W/m] HSAN IV transgenic model, we analyzed the expression of protein markers characterizing the main sensory neuron subtypes.
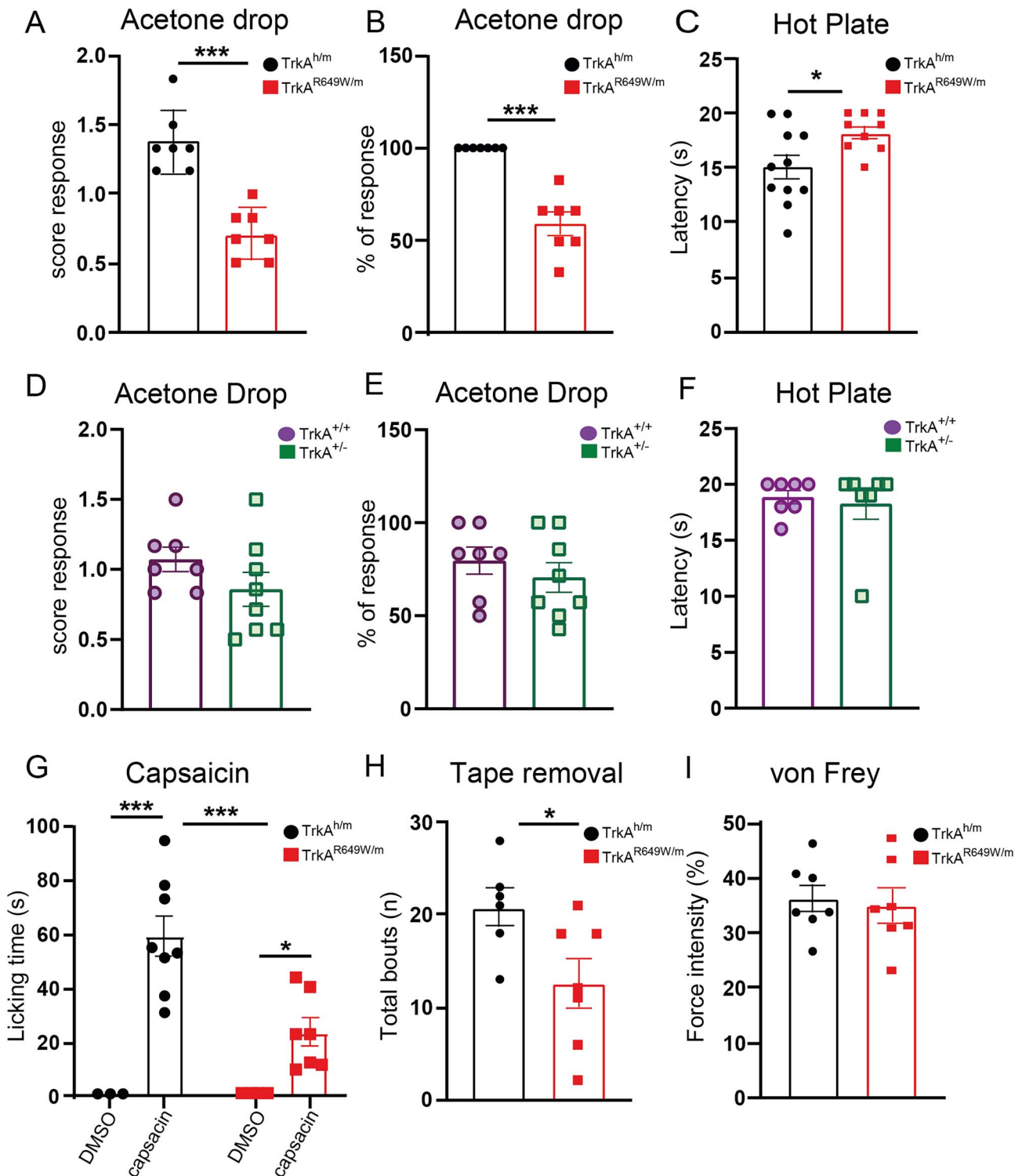
Figure 4. The R649W mutation specifically affects the response to noxious-thermal stimuli and the response to a mechanical innocuous stimulus. Comparable response to noxious thermal stimuli in TrkA$^{+/-}$ mice. (**A** and **B**) Decreased cold sensitivity of TrkA$^{R649W/m}$ mice, analyzed as score and percentage (%) of responses on six trials A: Student's *t* two-tailed test (*t* = 5.970, *P* ≤ 0.001); B: Mann–Whitney Rank Sum Test (*P* ≤ 0.001) *n* = 7 per group (**C**) Increased latency in TrkA$^{R649W/m}$ mice to respond to thermal stimulus of 48°C. Student's *t* two-tailed test (*t* = −1.281, *P* = 0.025); TrkA$^{h/m}$ *n* = 11; TrkA$^{R649W/m}$ *n* = 9. (**D** and **E**) Comparable response to cold sensitivity between TrkA$^{+/+}$ and TrkA$^{+/-}$, both in the score and percentage (%) of responses D: Student's *t* two-tailed test (*t* = 1.391, *P* = 0.188); E: Student's *t* two-tailed test (*t* = 0.831, *P* = 0.421); TrkA$^{+/+}$ *n* = 7 and TrkA$^{+/-}$ *n* = 8. (**F**) No differences between TrkA$^{+/+}$ and TrkA$^{+/-}$ in response to thermal stimulus of 48°C Mann–Whitney rank sum test (*P* = 0.902) *n* = 7 per group. (**G**) Decreased nociceptive behavior in TrkA$^{R649W/m}$ mice after intraplantar injection of capsaicin (9 $\mu g/\mu l$) compared to the control group. Two-way ANOVA (F$_{(1,18)}$ = 6.190, *P* = 0.023 followed by Holm-Sidak test (**P* = 0.032; ****P* ≤ 0.001); TrkA$^{h/m}$ *n* = 8; TrkA$^{R649W/m}$ *n* = 7. (**H**) Reduced number of bouts in response to a piece of adhesive tape applied to the back neck of HSAN IV mice, compared to controls. Student's *t* two-tailed test (*t* = 2.419, *P* = 0.034); TrkA$^{h/m}$ *n* = 6; TrkA$^{R649W/m}$ *n* = 7. (**I**) No differences between wild type and TrkA$^{R649W/m}$ mice in response to mechanical stimulation measured by von Frey test. Student's *t* two-tailed test (*t* = −0.274, *P* = 0.789); TrkA$^{h/m}$ *n* = 7; TrkA$^{R649W/m}$ *n* = 7. Data are presented as mean ± SEM.

First of all, no differences were found in the total DRG cell number between TrkA$^{R649W/m}$ and control mice (TrkA$^{h/m}$ 1182.53 cells/mm^2, TrkA$^{R649W/m}$ 1057.33 cells/mm^2; student's t two-tailed test $t = 1.396$ $P = 0.212$; $n = 4$ for both groups). We then investigated by immunofluorescence the number of neurons expressing the TrkA receptor and the transient receptor potential vanilloid 1 (TRPV1) (Fig. 5A and B). Quantification revealed a loss of TRPV1 expression in primary sensory neurons, whereas no differences were observed in the expression of TrkA. Moreover, the number of DRG neurons co-expressing TRPV1 and TrkA in TrkA$^{R649W/m}$ mice was reduced (Fig. 5E). Then, we examined the numbers of small-diameter neurons, divided into two main groups: the peptidergic calcitonin gene-related peptide (CGRP)-positive and non-peptidergic isolectin-B4 (IB4)-positive populations respectively (Fig. 5C and D). The number of neurons expressing CGRP was normal in TrkA$^{R649W/m}$ mice, whereas the numbers of IB4-positive CGRP/IB4 co-expressing neurons were strongly affected by R649W mutation (Fig. 5F).

We further investigated the neuronal subpopulations in DRGs from TrkA$^{R649W/m}$ mice, using known markers of proprioceptive sensory neurons and of non-nociceptive C-low-threshold mechanoreceptors (C-LTMRs) (Supplementary Material, Fig. S2). In addition to Neurofilament 200 (NF200), a marker of myelinated sensory neurons (60), we also used Parvalbumin (PV) as a marker of proprioceptors (60) (Supplementary Material, Fig. S2A and B), while unmyelinated c-LTMRs were identified using tyrosine hydroxylase (TH) (58) (Supplementary Material, Fig. S2C and D). We found no changes in the percentage of sensory neurons expressing PV-NF200 and TH-NF200 (Supplementary Material, Fig. S2E and F). Altogether, our data suggest that the R649W mutation specifically impacts the TRPV1+ and IB4+ subsets of DRG neurons, known to be essential for pain sensation, without affecting other neurons involved in mechanical or proprioceptive functions.

Severe lack of PGP9.5-positive fibers in the skin of TrkA$^{R649W/m}$ mice

In HSAN IV patients, the lack of pain sensation is associated with the loss of sensory afferents in the skin (26). For this reason, we investigated skin sensory innervation in TrkA$^{R649W/m}$ and control mice (Fig. 6A and C). The area and number of PGP9.5-immunoreactive terminals were decreased in the glabrous skin sections of TrkA$^{R649W/m}$ mice compared to control mice (Fig. 6B). In addition, we observed a diminished innervation in the hairy skin of TrkA$^{R649W/m}$ mice (Fig. 6D). In agreement with the clinical features of HSAN IV disease, TrkA$^{R649W/m}$ mice show a severe lack of innervation in both glabrous and hairy skin.

Sympathetic innervation of internal organs is not affected by TrkA^{R649W} mutation

Among NGF-target tissues, the sympathetic nervous system is one of the most influenced by the NGF–TrkA system. We have evaluated the sympathetic innervation of internal organs, such as the stomach, heart and kidneys of HSAN IV TrkA$^{R649W/m}$ mice compared to control animals (Supplementary Material, Fig. S4). No significant differences were detectable by whole-mount immunofluorescence of the organs suggesting that TrkA^{R649W} mutation does not directly affect the sympathetic innervation of such organs. Further studies may be necessary to comprehensively understand the link between the mutant TrkA and the sympathetic nervous system.

Anhidrosis in TrkA^{R649W} but not in HSAN V NGF$^{R100W/m}$ mice: a distinctive hallmark of HSAN IV disease

The absence of sweating is a distinctive clinical trait of HSAN IV patients (26), unlike HSAN V patients, which harbor mutations in the *NGF* gene (25,61). For this reason, by using a pilocarpine-induced sweat assay (62), we examined if TrkA$^{R649W/m}$ mice were affected by abnormalities in sweat production. Having recently developed an HSAN V mouse model (NGF$^{R100W/m}$) (63,64), we had the opportunity to compare the sweating phenotype in heterozygous HSAN IV TrkA$^{R649W/m}$ and HSAN V NGF$^{R100W/m}$ mice (NGF$^{R100W/m}$), in order to evaluate the specific response of an HSAN IV mouse model in this specific assay. In the pilocarpine-induced sweat assay, sweating appears as dark precipitates on iodine and starch-coated footpads (Fig. 7A). After pilocarpine injection, the formation of dark spots in footpads was monitored and recorded by a digital camera at 2, 5 and 10 min. The iodine-starch sweat test revealed striking anhidrosis in TrkA$^{R649W/m}$ mice as also shown in representative pictures (Fig. 7B). On the other hand, the sweat assay performed in NGF$^{R100W/m}$ and their corresponding control mice revealed no differences in the number of black spots, confirming normal sweating in the HSAN V mouse model and further validating the specificity of our HSAN IV model (Fig. 7C). This is fully consistent with human studies reporting sweating alterations in HSAN IV but not in HSAN V patients.

Since sweat glands are innervated with adrenergic and cholinergic terminals, we investigated if reduced sweating was associated with an altered sympathetic innervation of these populations. The area occupied by TH-immunoreactive positive fibers appeared normal in both TrkA$^{R649W/m}$ and controls, as well as in HSAN V sweat glands (Fig. 7D–E). No differences were also found in the mean immunofluorescence signal intensity of the cholinergic fibers labeled with the vesicular acetylcholine transporter (VAChT) between TrkA$^{R649W/m}$ and controls, as well as in HSAN V mice (Fig. 7F and G). We can conclude that the differential anhidrosis sweating phenotype, observed in HSAN IV versus HSN V mice is not due to a differential innervation of the adrenergic and cholinergic innervation of sweat glands in the two mouse lines.

Impaired cognitive abilities and reduced sociability in TrkA$^{R649W/m}$ but not in NGF$^{R100W/m}$ mice

Another distinctive feature of HSAN IV patients is the presence of mental retardation with variable severity (36), which include aspects that have been classified as attention deficit hyperactivity disorder (ADHD) (65). Thus, to evaluate cognitive abilities in TrkA$^{R649W/m}$ mice, we performed a battery of tests that have been often used in mouse models of ADHD to evaluate working spatial memory and inattention, anxiety and sociability (66,67). First, we tested the tendency of rodents to alternately explore new environments, reproduced by the arms of the Y-maze. The spontaneous alternations evaluated in Y-maze apparatus were reduced in TrkA$^{R649W/m}$ mice compared to the control group (Fig. 8A). In addition, when tested in an elevated plus maze, TrkA$^{R649W/m}$ mice exhibited less anxious behavior than control mice (Fig. 8B). Importantly, these alterations in both Y-maze and elevated plus maze test were not detected in TrkA$^{+/-}$ mice (Fig. 8C and D), suggesting that these behavioral impairments are strictly related to the R649W mutation. In the novel object recognition test, in which a specific form of
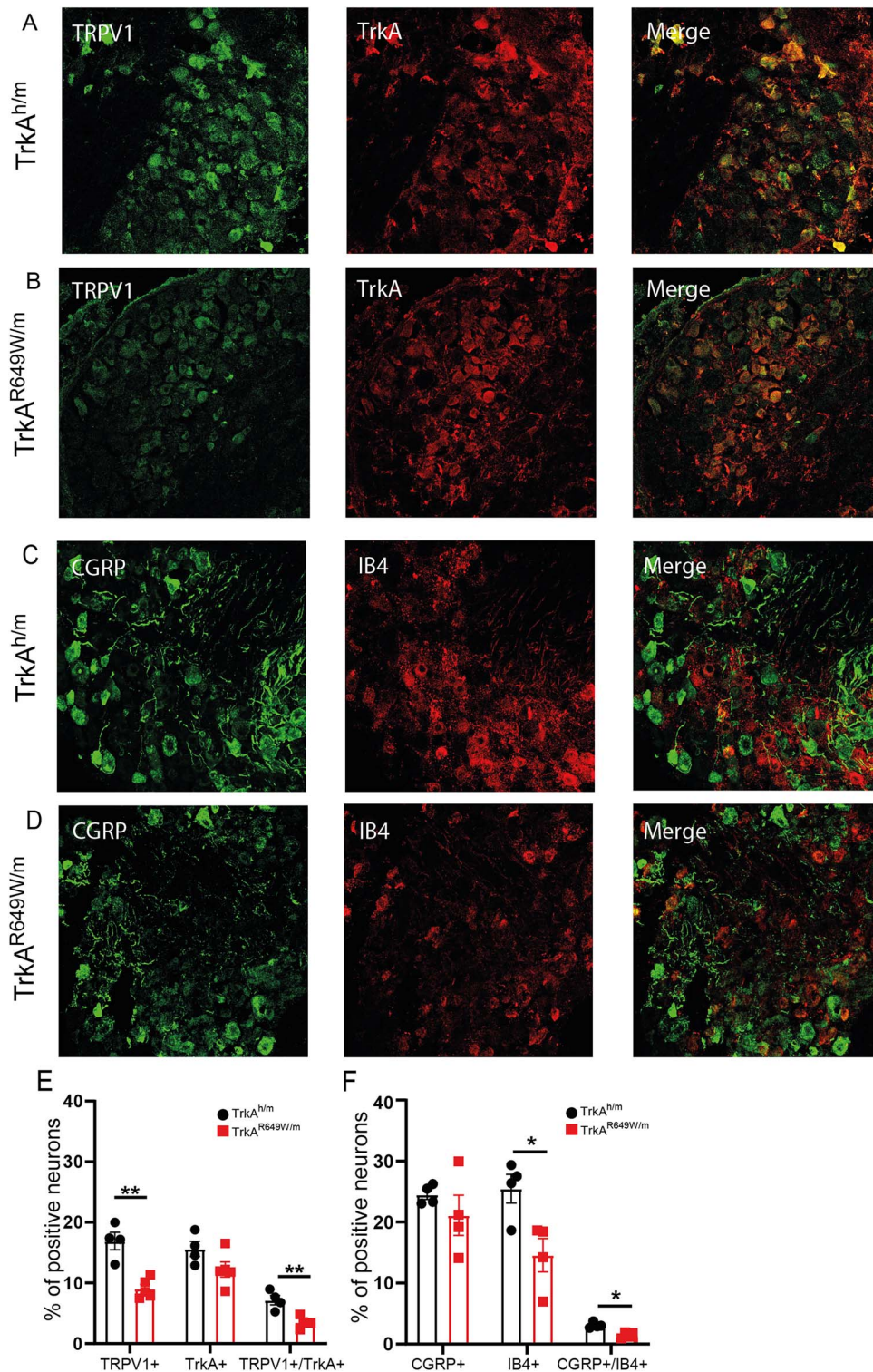
Figure 5. Analysis of nociceptive markers in DRG: reduced expression of TRPV1 and IB4 expression. (**A–D**) Double immunofluorescence of DRG cryosections: for (A and B) TRPV1 and TrkA, (C and D) CGRP and IB4. (**E**) Significant decrease of TRPV1+/TrkA+ sensory neurons in TrkA$^{R649W/m}$ mice. Student's *t* two-tailed test: TRPV1 $t = 5.207$, $P = 0.001$; TrkA $t = 1.881$, $P = 0.102$; TRPV1/TrkA $t = 4.456$, $P = 0.003$; TrkA$^{h/m}$ $n = 4$, TrkA$^{R649W/m}$ $n = 5$). (**F**) Reduced number of IB4-positive neurons in TrkA$^{R649W/m}$ mice. Student's *t* two-tailed test: CGRP $t = 1.089$, $P = 0.318$; Mann–Whitney rank sum test: IB4 $P = 0.03$; Student's *t* two-tailed test CGRP/IB4 $t = 4.933$, $P = 0.003$; TrkA$^{h/m}$ $n = 4$, TrkA$^{R649W/m}$ $n = 4$.

learning and memory abilities is assessed, no differences were found between TrkA$^{R649W/m}$ mice and their controls (Fig. 8E).

Another hallmark of HSAN IV patients is an altered social interaction and the propensity to avoid eye contact (68). To investigate the effect of R649W mutation on social behavior, we tested the

performance of HSAN IV mice in the three-chamber sociability test (69,70). During the socialization phase, TrkA$^{R649W/m}$ mice displayed a comparable exploration time between the unfamiliar mouse cage (namely stranger 1—S1) and the inanimate object cage, indicating altered sociability compared to controls (Fig. 9A,
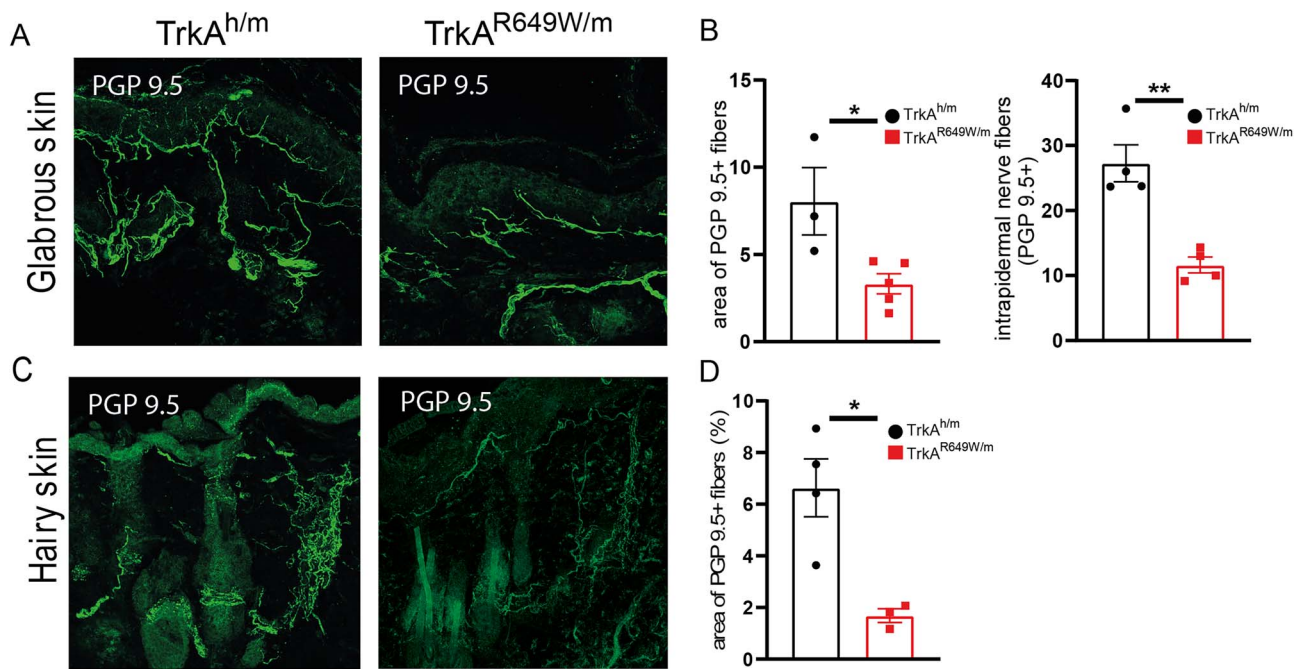
Figure 6. Loss of innervation in hairless and hairy skin in TrkA$^{R649W/m}$ mice. (**A**, **C**) Representative images and (**B**, **D**) quantification of PGP9.5 expression in glabrous and hairy skin sections. (B) Left: significant reduction of hairless skin innervation measured as the area occupied by PGP9.5-positive fibers. Student's t two-tailed test: $t = 2.947$ $P = 0.026$ TrkA$^{h/m}$ $n = 3$, TrkA$^{R649W/m}$ $n = 5$. Right: reduction of PGP9.5-postive intraepidermal fibers in TrkA$^{R649W/m}$ compared to TrkA$^{h/m}$ mice. Student's t two-tailed test: $t = 5.045$ $P = 0.002$ TrkA$^{h/m}$ $n = 4$, TrkA$^{R649W/m}$ $n = 4$. (D) TrkA$^{R649W/m}$ mice exhibit a diminished hairy skin innervation measured as the area occupied by PGP9.5-positive fibers. Student's t two-tailed test: $t = 3.670$ $P = 0.014$ TrkA$^{h/m}$ $n = 4$, TrkA$^{R649W/m}$ $n = 3$.

left) while, as expected, HSAN V NGF$^{R100W/m}$ mice and wild-type mice, showed a significant preference for the mouse cage rather than the object (Fig. 9A, right). When tested in the social novelty preference test, in which a new unfamiliar mouse (namely Stranger 2—S2) replaced the object into the wire cup, TrkA$^{R649W/m}$ mice, compared to TrkA$^{h/m}$ mice, do not show a significant preference for the unfamiliar S2 mouse (Fig. 9B, left). Interestingly, we found that sociability was unaltered in NGF$^{R100W/m}$ mice (Fig. 9B, right), suggesting that this characteristic behavior is strictly related to the HSAN IV clinical phenotype, as reported in human patients.

Our comprehensive array of behavioral tests shows that TrkA$^{R649W/m}$ mice are characterized by deficits in working memory, reduced anxiety and decreased social interactions.

Overall, we report that our TrkA$^{R649W/m}$ mice recapitulate key phenotypes associated with HSAN IV disease and thus they could represent an important model for studying pain insensitivity.

Discussion

Pain is a universal warning system that has evolved to prevent and avoid injuries. The nociceptive system is thus highly conserved in all animal species and requires specialized primary sensory neurons that are responsive to a wide variety of noxious stimuli. Among the different signaling mechanisms that underlie pain perception, a key role is played by TrkA (71,72). Indeed, a subpopulation of sensory neurons called peptidergic-nociceptors are NGF-dependent and express TrkA receptors (73). Consistently, mice deprived of the NGF–TrkA signaling during embryonic life fail to develop sensory neurons properly, thus losing their response to noxious stimuli (54,74). The necessity of a functioning NGF–TrkA system strikingly emerges also from the existence of two rare genetic conditions of pain insensitivity called HSAN IV and V that

affect TrkA and NGF, respectively (32,75). In particular, HSAN IV is due to mutations in the *TRKA* gene (*NTRK1*) and it is specifically characterized by the loss of pain sensation, anhidrosis and variable degree of mental retardation (36). Genetic analyses of HSAN IV patients have identified more than 100 mutations in *TRKA* (HGMD 2021.4), suggesting that mutations in TrkA functional domains, such as TKD, can correlate with more severe clinical manifestations (26,76). Nowadays, no suitable animal model for HSAN IV has yet been developed, making the search for disease-relevant biomarkers and the development of therapeutic strategies, particularly challenging. In this work, we have studied *in vitro* and *in vivo* the contribution of a specific HSAN IV mutation, Arg649Trp (R649W), located in the TKD of *TRKA* (28). It had been previously shown that the substitution of the Arginine-649 residue causes a strong reduction in the receptor phosphorylation in response to the binding of NGF (28–30). To build and expand on existing literature, *in vitro* we first demonstrated that the R649W mutation prevents the auto-phosphorylation resulting in the inactivation of the receptor without affecting the total amount of protein. Interestingly, we also found that the TrkA^{R649W}-inactive receptor shows a lower level of ubiquitination compared to TrkA^{WT}. Thus, arginine-substitution R649W in the TKD results important for the constitutive ubiquitination of TrkA, suggesting a potential relevance in the TrkA trafficking (77). Furthermore, using TIRF microscopy combined with SPT, we observed reduced membrane mobility of TrkA^{R649W}, possibly dependent on the kinase inactivity of TrkA and, surprisingly, a significant increase in the membrane density of TrkA^{R649W}. The mobility of the TrkA receptor is not only NGF-dependent (50), but mutations in TKD, such as R649W, could be sufficient to modify the receptor-membrane dynamics. Our *in vitro* data indicate that the altered molecular characteristic and trafficking of TrkA^{R649W} protein could be the underlying mechanism affecting pain sensitivity in HSAN IV
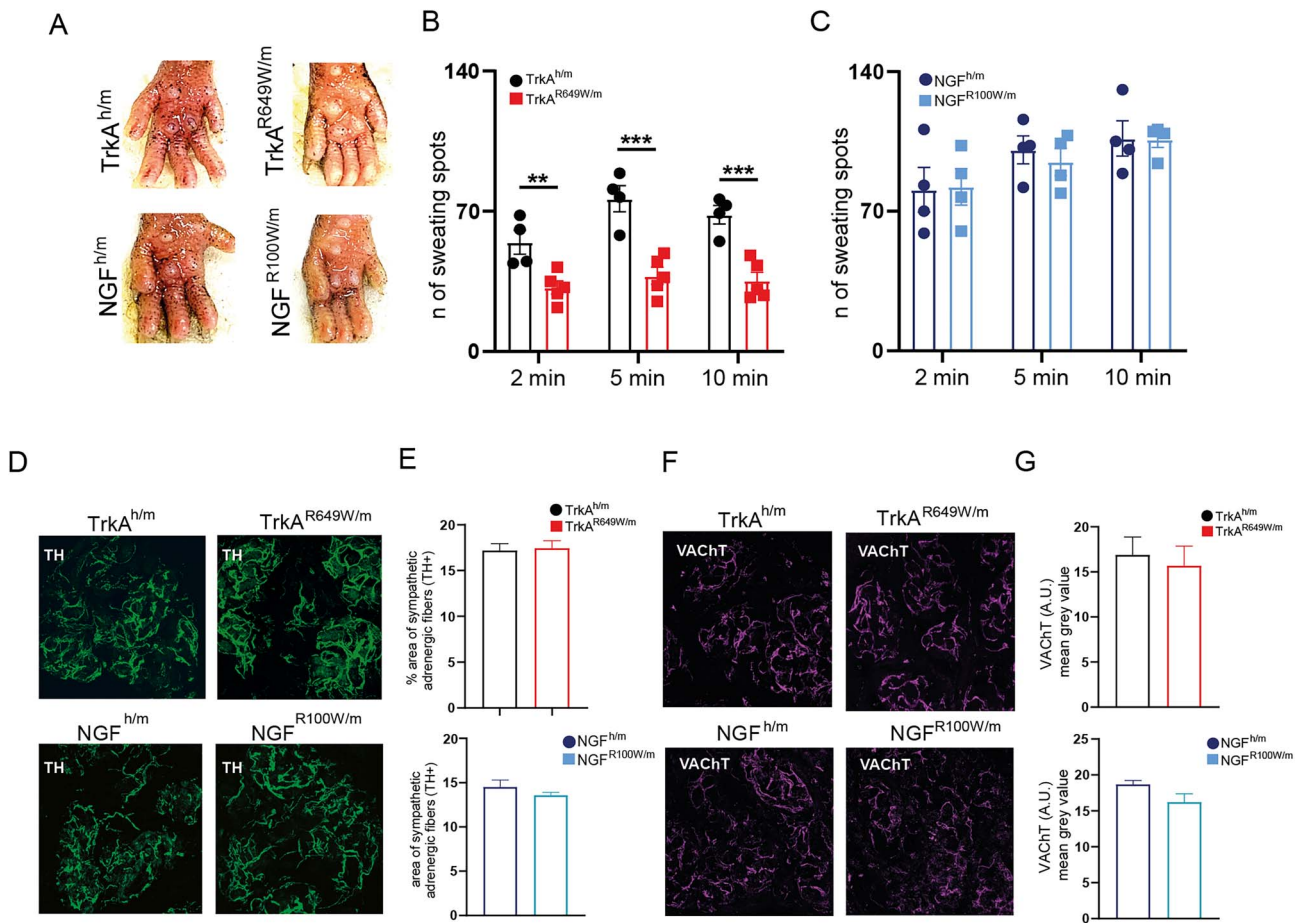
Figure 7. Impaired sweating in HSAN IV TrkA$^{R649W/m}$ but not in HSAN V NGF$^{R100W/m}$ mice. (**A**) Representative images of sweat droplets (dark precipitates from iodine/starch assay) on footpads at 5 min and quantification of sweat droplets at 2, 5 and 10 min. (**B**) TrkA$^{R649W/m}$ mice show a significant reduction in the number of sweat droplets compared to control mice. Two-way RM ANOVA ($F_{(2,14)} = 2.61$ $P = 0.109$), followed by Holm-Sidak test: 2 min $P = 0.005$; 5 min $P \leq 0.001$; 10 min $P \leq 0.001$; TrkA$^{h/m}$ $n = 4$, TrkA$^{R649W/m}$ $n = 5$. (**C**) Normal sweating in NGF$^{h/m}$ and NGF$^{R100W/m}$ Two-way RM ANOVA ($F_{(2,12)} = 0.084$ $P = 0.920$), followed by Holm-Sidak test: 2 min $P = 0.940$; 5 min $P = 0.652$; 10 min $P = 0.821$; NGF$^{h/m}$ $n = 4$, NGF$^{R100W/m}$ $n = 4$). (**D**) Representative images showing the innervation of sweat glands in the footpad, revealed by TH immunofluorescence. (**E**) Unaffected sympathetic innervation of sweat glands in TrkA$^{h/m}$ and TrkA$^{R649W/m}$ mice and in NGF$^{h/m}$ and NGF$^{R100W/m}$. TrkA$^{h/m}$ and TrkA$^{R649W/m}$ Student's t two-tailed test $t = -0.228$, $P = 0.826$; TrkA$^{h/m}$ $n = 5$, TrkA$^{R649W/m}$ $n = 4$. While, NGF$^{h/m}$ and NGF$^{R100W/m}$ Student's t two-tailed test $t = 1.116$, $P = 0.297$ $n = 5$ per group. (**F**) Representative images showing the sympathetic innervation of sweat glands, revealed by VAChT immunofluorescence. (**G**) VAChT (A.U) mean gray value revealed no differences of sympathetic innervation in TrkA$^{h/m}$ and TrkA$^{R649W/m}$ mice and in NGF$^{h/m}$ and NGF$^{R100W/m}$. Histograms summarize the mean immunofluorescence signal intensity measured as the subtraction of the mean gray values and the background. TrkA$^{h/m}$ and TrkA$^{R649W/m}$ Student's t two-tailed test $t = 0.411$, $P = 0.702$; TrkA$^{h/m}$ $n = 3$, TrkA$^{R649W/m}$ $n = 3$. While, NGF$^{h/m}$ and NGF$^{R100W/m}$ Student's t two-tailed test $t = 1.924$, $P = 0.127$ $n = 3$ per group.

patients. Recently, structural mapping of HSAN IV TrkA variants indicates that mutations located in TKD can affect the TrkA interaction with substrates, such as PLCγ, and damages in TrkA-PLCγ interactions may have an analgesic effect on pain states in mice (41). In this regard, we recently generated PC12 cell lines lacking one or both NGF receptors using CRISPR/Cas9 (13), which provide a genetically clean background for the expression of TrkA^{R649W} to study the specific signaling features.

Having established the main *in vitro* properties of the HSAN IV TrkA^{R649W} mutant, we generated TrkA$^{R649W/m}$ mice. In homozygosity, the R649W TrkA mutation causes a postnatal lethal phenotype within the first week of life. The lethality observed for homozygous TrkA$^{R649W/R649W}$ mice is only seemingly in contrast with the homozygosity of the R649W mutation in HSAN IV patients (28). In fact, individuals affected by HSAN IV often survive into adulthood also thanks to careful medical treatments (32). Moreover, this was quite expected due to the observed lethality also in TrkA$^{-/-}$ mice (54) and possibly underlies redundant

mechanisms that have developed during evolutionary processes for the NGF–TrkA pathway in humans. Thus, in order to understand the physiological correlates of the TrkA^{R649W} mutation, we have characterized in depth the heterozygous TrkA$^{R649W/m}$ mice. In line with HSAN IV human symptoms, TrkA$^{R649W/m}$ mice failed to react to thermal and chemical noxious stimuli. We found a diminished licking behavior after capsaicin injection consistent with pain insensitivity in TrkA$^{R649W/m}$ mice, and interestingly, we observed a decrease in the number of TRPV1+ neurons that are involved in the mediation of noxious stimuli. The loss of TRPV1+ neurons, crucial in avoiding tissue damage and in the development of NGF-induced heat hyperalgesia (42,78), and the behavioral correlate of pain insensitivity in HSAN IV TrkA$^{R649W/m}$ mice, may represent a feasible explanation for the inability of HSAN IV patients to avoid injuries caused by noxious-thermal stimuli. TrkA$^{R649W/m}$ mice also show a decreased reaction to cold, which might suggest an abnormal regulation of the cold-activated channels TRPA1, expressed in subsets of heat-sensitive,
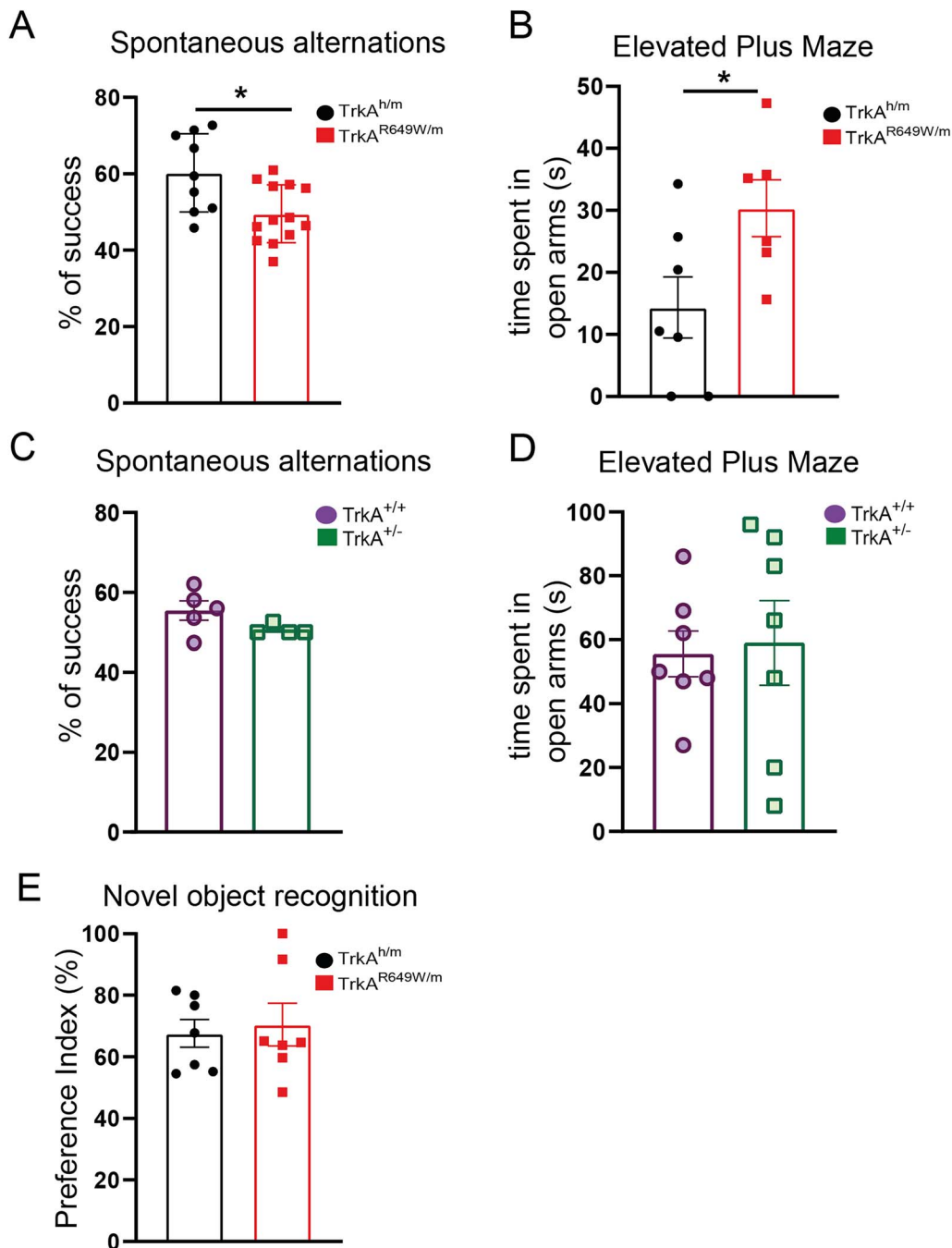
Figure 8. Impaired cognitive abilities in TrkA$^{R649W/m}$ mice and not in TrkA$^{+/-}$ mice. (**A**) Decreased percentage (%) of success in Y-maze test in TrkA$^{R649W/m}$ mice. Student's *t* two-tailed test, ($t = 2.519$, $P = 0.026$), TrkA$^{h/m}$ $n = 8$, TrkA$^{R649W/m}$ $n = 7$. (**B**) Decrease of anxiety-related behavior in HSAN IV mice, evaluated in the elevated plus maze. Student's *t* two-tailed test, ($t = -2.349$, $P = 0.039$); TrkA$^{h/m}$ $n = 7$, TrkA$^{R649W/m}$ $n = 6$. (**C, D**) Percentage (%) of success in Y-maze test (C) and anxiety-related behavior (D) are not affected in both TrkA$^{+/+}$ and TrkA$^{+/-}$ mice. C: Student's *t* two-tailed test ($t = -1.683$, $P = 0.136$); TrkA$^{+/+}$ $n = 5$ and TrkA$^{+/-}$ $n = 4$; D: Student's *t* two-tailed test ($t = -0.229$, $P = 0.823$) $n = 7$ per group. (**E**) No differences in the novel object recognition test (Student's *t* two-tailed test, $t = 0.351$, $P = 0.732$; $n = 7$ per group).

TRPV1-positive and NGF-dependent neurons (79–82). Thus, the lack of thermal hyperalgesia is linked to the hypofunctionality of TrkA^{R649W} receptor, as found in rodent species such as the naked mole-rat, which naturally displays pain insensitivity (78). We also found a significant decrease in IB4+ neurons in DRG of TrkA$^{R649W/m}$ mice. Overall, our data reinforce the importance of a functional TrkA system in DRG development and function, but whether the observed changes are due to a developmental defect, or to a failure of adult maintenance of these neurons, remains to be investigated. Interestingly, though

the pain-related behavioral phenotype of TrkA$^{R649W/m}$ mice is quite similar to that of HSAN V NGF$^{R100W/m}$ mice (64), only HSAN IV TrkA$^{R649W/m}$ mice show a specific lack of the IB4+ DRG subpopulation. Thus, the developmental consequences of the HSAN IV TrkA^{R649W} mutation on sensory neurons appear to be more severe than those observed in HSAN V mice (64), possibly identifying different contributions of the receptor and the ligand to the development of sensory neurons. The inability of TrkA$^{R649W/m}$ mice to perceive thermal and chemical noxious stimuli was also accompanied by a strong reduction
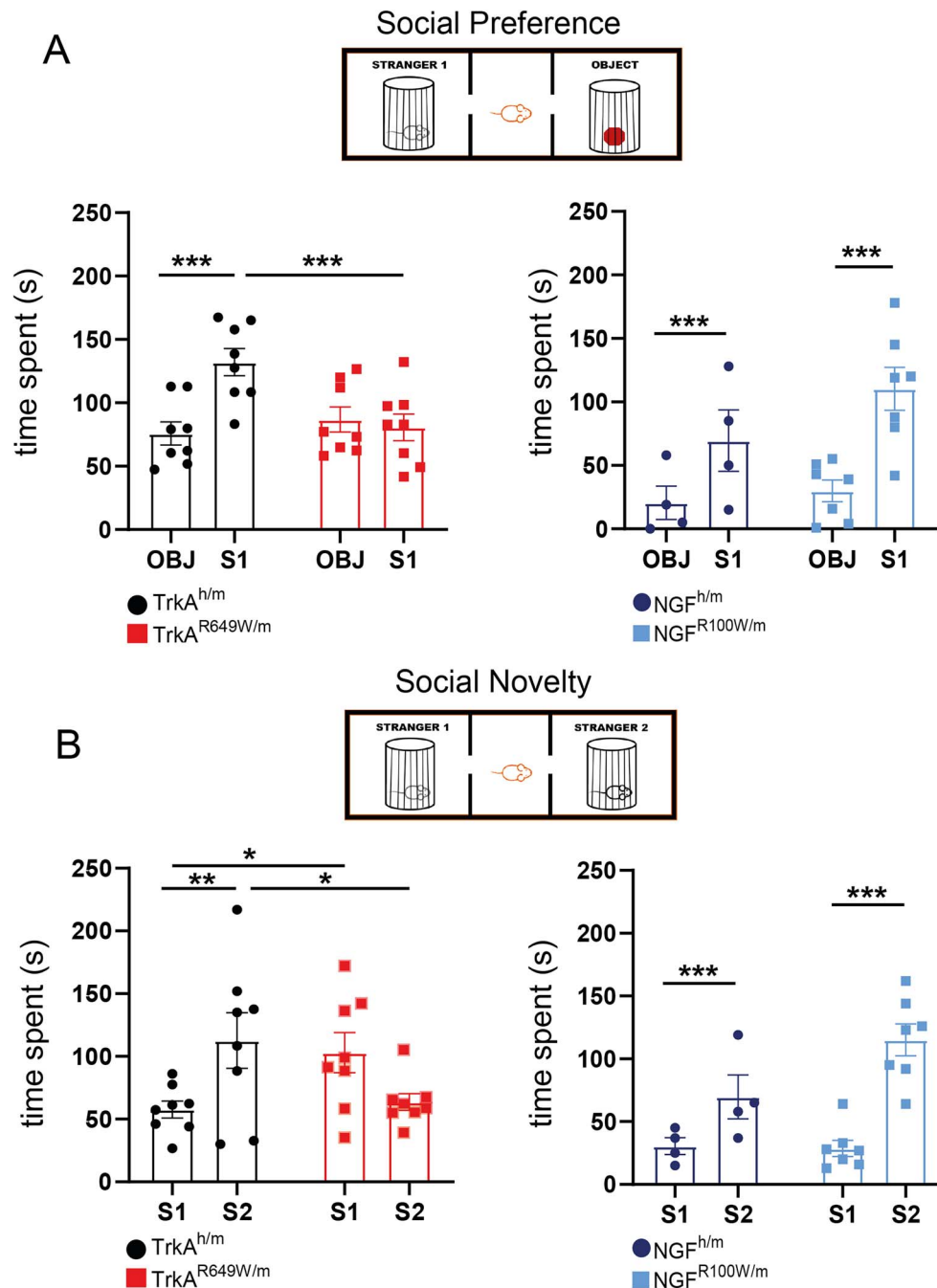
Figure 9. **Reduced sociability in TrkA^R649W/m and not in NGF^R100W/m mice.** (**A**) Left: TrkA^R649W/m mice display reduced social preference in three-chamber test. Two-way ANOVA ($F_{(1,28)} = 9.56$ $P = 0.004$), followed by Holm-Sidak method ***$P \leq 0.001$ TrkA^h/m $n = 8$, TrkA^R649W/m $n = 8$. Right: no differences in social preference in the HSAN V mouse model. Two-way ANOVA ($F_{(1,18)} = 9.37$ $P = 0.346$), ***$P \leq 0.001$ NGF^h/m $n = 4$, NGF^R100W/m $n = 7$. (**B**) Left: Social novelty behavior is impaired in TrkA^R649W/m mice Two-way ANOVA ($F_{(1,28)} = 10.63$ $P = 0.003$), followed by Holm-Sidak method **$P = 0.012$; *$P = 0.035$; *$P = 0.023$ TrkA^h/m $n = 8$, TrkA^R649W/m $n = 8$. Right: normal social novelty exploration in NGF^h/m and NGF^R100W/m Two-way ANOVA, ($F_{(1,18)} = 4.01$ $P = 0.060$) ***$P \leq 0.001$ NGF^h/m $n = 4$, NGF^R100W/m $n = 7$.

of cutaneous innervation in both hairless and hairy skin, possibly due to early events in sensory neuron development (83). Interestingly, TrkA^R649W/m mice also display a reduced response to non-noxious mechanical stimulation in the hairy skin, which is known to depend on NGF–TrkA signaling (59). Since efficient TrkA trafficking and signaling are necessary for the innervation of NGF-target organs by sensory neurons (84,85), it is tempting to hypothesize that the reduced skin innervation is connected to the altered TrkA^R649W trafficking observed *in*

vitro. In fact, dysregulation of TrkA axonal trafficking has been causally linked to peripheral neuropathies (86) and to diminished nociceptive responses (47,87). A similar painless phenotype is also found in patients affected by familial dysautonomia (FD) or HSAN III/Riley-Day syndrome, caused by mutations in *ELP1/IKBKAP* gene that lead to the accumulation of DNA damages in differentiated TrkA+ neurons (88,89). As found in Elp1-deficient mice, the lack of Elp1 impairs the retrograde transport of NGF in sensory neurons (90,91), suggesting that

mutations in ELP1, as well as in the TrkA gene, might have a partially common consequence in the physiology of sensory neurons.

One distinctive trait of human HSAN IV patients is their inability to sweat normally (26). By using a murine-adapted version of Minor's starch iodine test (92), we determined in our transgenic model the presence of anhidrosis, a distinctive trait of HSAN IV disease linked to thermoregulation deficits. We show a lack of anhidrosis in TrkA$^{R649W/m}$ mice highlighting yet again the specificity of our HSAN IV model. Moreover, histological analysis of sweat glands of TrkA$^{R649W/m}$ mice revealed no differences compared to controls. The innervation of sweat glands appears to be variable among HSAN IV patients. Skin biopsies in some patients revealed normal sweat glands innervation (35,93,94), while skin samples of other patients reported non-innervated sweat glands (95,96). Although our results suggest no differences in the sweat glands' innervation, we cannot exclude electrophysiological alterations and future studies aimed at examining both sensory and sympathetic nerve conduction might be useful to complete the HSAN IV understanding. However, based on our results and observations, we suggest that a possible cause of anhidrosis in HSAN IV might be found in brain regions, such as the preoptic hypothalamic area, that control thermoregulation (97). How thermoregulatory processes are integrated in the brain of HSAN IV patients and TrkA^{R649W} mice, and how this leads to anhidrosis will need to be clarified in future work.

In addition to the literature on heterozygous TrkA$^{+/-}$ mice (98), our results on sweat glands and internal organs suggest that the sympathetic system is by and large not affected by the TrkA^{R649W} mutation and a possible explanation can be found during the early stages of the development of some sympathetic neurons that are dependent on GDNF-Ret signaling instead of NGF–TrkA signaling (99–101).

HSAN IV is also characterized by mental retardation and cognitive deficits (75) reportedly similar to ADHD (65). Behavioral tests revealed cognitive impairments in TrkA$^{R649W/m}$ mice, as well as general sociability and interest in social novelty, suggesting a key role of the TrkA^{R649W} in cognitive performance. In fact, difficulty in establishing interpersonal relationships is considered an exclusive trait of children with HSAN IV (32).

In conclusion, by exploiting suitable control animal models such as HSAN V NGF$^{R100W/m}$ (64) and TrkA$^{+/-}$ mice (54), we have demonstrated that HSAN IV TrkA$^{R649W/m}$ mice mimic the clinical phenotype of HSAN IV patients and they can be considered an experimental platform to explain the clinical aspect of HSAN IV disease. Moreover, our results suggest unexplored roles of TrkA in thermoregulation and sociability and offer promising new routes for testing future therapies. The development of this transgenic animal model can strongly help to broaden the knowledge about the causes, onset and progression of HSAN IV and could provide new knowledge about how the NGF–TrkA signaling affects both nociception and pain perception, in order to isolate new candidates for the development of innovative therapeutic strategies to alleviate chronic pain.

Materials and Methods
Plasmids for TrkA^{WT} and TrkA^{R649W} expression in cultured cells

Human TrkA^{WT} cDNA sequence (isoform II) in pReceiver-M03 (OmicsLink, ImaGenes, Berlin) was subcloned in pcDNA3.1 plasmid (Invitrogen). The mutation R649W was obtained starting from wild type sequence in pCDNA3.1, using the QuikChange site-directed mutagenesis kit (Agilent) and a pair of specific primers (Forward: CAT TTT GTG CAC TGG GAC CTG GCC ACA CGC; Reverse: GCG TGT GGC CAG GTC CCA GTG CAC AAA ATG). pCDNA3.1-human TrkA^{WT} and pCDNA3.1-human TrkA^{R649W} plasmids were transfected in Hek293 cells to perform western blot (WB) and ubiquitination assay described below.

The cloning to obtain S6-tagged human TrkA cDNA sequence in an 'all-in-one' third-generation Tet-on lentiviral pTRE vector has been described previously (49,102). This construct was used to generate S6-tagged human TrkA^{R649W} mutant, using QuikChange site-directed mutagenesis kit (Agilent) and the same pair of primers reported in the paragraph above. The mutant clone (S6-tagged TrkA^{R649W}) was checked by DNA sequencing and used for the transduction of immortalized and primary cells.

Cell culture and dorsal root ganglion neuron primary cultures

SK-N-BE (2) (ATCC® CRL-2271™) and SH-SY5Y (ECACC 94030304) cell lines were grown in Dulbecco's Modified Eagle Medium (DMEM)/F-12 medium supplemented with 10% fetal bovine serum, 1% penicillin–streptomycin, 1% L-glutamine and 25 mM HEPES. HEK293T/17 cells (ATCC® CRL-11268™) were grown in DMEM high-glucose (4.5 g/l) medium supplemented with 10% fetal bovine serum, 1% penicillin–streptomycin, 1% L-glutamine, 1% sodium pyruvate. DRG neurons were prepared from neonatal (P3–P4) wild type mice, by following the protocol described in (51,64), and plated onto coverslips coated with 30 μg/ml poly-D-lysine (Sigma-Aldrich) and 2 μg/ml laminin (Thermofisher). Dissected neurons were maintained on coverslips in primary neuron basal medium (PNBM, Lonza) supplemented with 1% L-glutamine (Lonza), 0.1% gentamicin sulfate/amphotericin-B (Lonza), 2% NSF-1 (Lonza) and 50 ng/ml of mouse NGF. Twenty-four hours after seeding, 2.5 μM cytosine β-d-arabinoside (AraC, Sigma) was added for inhibition of glia proliferation. Neuronal culture medium was changed every 3–4 days, removing about 1/3 of the volume and substituting it with warm, fresh neuron growth medium.

Western blot

Hek293 cells were transfected with pCDNA3.1-human TrkA^{WT} and pCDNA3.1-human TrkA^{R649W} plasmids following the manufacturer's instructions for Invitrogen Lipofectamine 2000 (Thermo Fisher Scientific). Forty-eight hours of transfection, Hek293 cells were stimulated with NGF^{WT} (100 ng/ml) for 30 min or maintained in basal conditions and then lysed in radioimmunoprecipitation assay (RIPA) buffer. Equal amounts of cell extracts were resolved by SDS-PAGE (10%), transferred on nitrocellulose membranes and probed overnight with primary antibodies: anti-TRKA (1:1000, Cell Signaling #2505), anti-phospho-TRKA (1:1000, Cell Signaling #9141), anti-Tubulin (1:10 000, Sigma #T6074). The primary antibody was detected using an appropriate secondary antibody. To analyze the state of ubiquitination of TrkA, samples were subjected to WB using an anti-Ubiquitin (1:500, Santa Cruz P4D1) antibody that detects both poly- and mono-ubiquitinated proteins. The signal was revealed with ECL solutions (BioRad) and acquired using a ChemiDoc system (BioRad). The optical density was quantified using the ImageJ software (NIH).

Viral transduction of immortalized and primary cells

Lentiviral particles containing S6-tagged TrkA^{WT} or S6-tagged TrkA^{R649W} were produced and concentrated following the

procedure described in Gobbo *et al.* (103). One day before transduction, about 0.8×10^5 of SK-N-BE neuroblastoma cells (ATCC) were seeded in a 30 mm-diameter culture dish and incubated at 37°C, 5% CO_2. On the day of transduction, after the removal of all culture medium and two washes with PBS (supplemented with 1 mM $CaCl_2$, 0.5 mM $MgCl_2$), 0.36 ml of non-supplemented DMEM/F12 medium containing 35 μl of concentrated viral stock ($1–2.5 \times 10^7$ infection-forming units per ml) and 4 μg/ml polybrene (Sigma-Aldrich) was added to the cultures. Cells were incubated at 37°C, 5% CO_2 for 1 h. Then, the infection medium was replaced with complete neuroblastoma cell medium to allow the transgene integration for at least 48 h. Cells were then split and seeded in Willco glass-bottom dishes for cell imaging and TrkA expression was induced by adding 0.05 ug/ul doxycycline in the cell medium.

For the transduction of neurons, the day after their plating 0.5 ml of warm PNBM supplemented with 4 μg/ml polybrene was prepared and mixed with 35 μl of concentrated viral stock. Then, the solution was vortexed for a few seconds to mix the viral particles. The medium was carefully removed from neuron cultures seeded on coated coverslips in 24-well plates, the solution containing the virus was added to each well, and incubated at 37°C in a 5% CO_2 humidified chamber for 2 h. Then, the infection medium was removed and fresh PNBM supplemented with 50 ng/ml of mouse NGF and 2.5 μM Ara-C was added. Cells were maintained at 37°C under 5% CO_2 humidified atmosphere for 48 h. Then transgene expression was induced by adding 1 μg/ml doxycycline for additional 24 h before performing the experiment.

Single molecule Q-dot labeling of surface TrkA in SK-N-BE cells

Forty-eight hours after the transduction, SK-N-BE cells were starved at 37°C for 2 h. Then, surface receptors were labeled with Qdot as described in (49). Briefly, cells were first biotinylated with 0.5% BSA, 1 μM Sfp synthase, 10 mM $MgCl_2$ and 2 μM of coA-biotin in starvation medium, for 30 min at 37°C. After two washes in PBS, cells were incubated for 2 min at room temperature (RT) with 2 nM Qdot® 655 streptavidin conjugate (Invitrogen) in borate buffer pH 8.3, 0.5% BSA and 215 mM sucrose. Cells were washed with PBS and left in medium. Finally, cells were stimulated with 125 ng/ml NGF or maintained in starvation medium. The addition of NGF was performed directly on the dish at the microscope, and cells were imaged for a maximum of 15 min upon ligand addition.

Total internal reflection fluorescence imaging

Cells prepared as described above were imaged at 37°C, 5% CO_2 with a Leica DM6000 microscope equipped with a TIRF-AM module, incubator chamber, electron multiplying charge-coupled-device (CCD) camera (ImagEM C9100-13, Hamamatsu), and 100× oil immersion objective (NA 1.47). For live-cell imaging, time series were acquired on a region of interest (ROI) with a constant size of 32.7×34.5 μm within the basal membrane of each cell. Qdot655 was imaged using the 488 nm laser line, FF01655/15 Semrock emission filter and a penetration depth of 110 nm. The integration time per frame, corresponding to the lag time between two consecutive frames, was set at 21 ms and typical time series lasted 3000 frames. The analysis of TrkA membrane dynamics was performed as reported in (50). We also quantified the density of spots corresponding to labeled membrane receptors by manually counting them and dividing this number for the basal cell membrane area.

Single molecule internalization assay

The single molecule internalization assay of TrkA-WT versus TrkA-R649W mutant transduced in SHSY5Y cells was performed as previously described (49). Briefly, cells seeded in glass-bottom WillCo dishes were starved for 2 h, receptors labeled with Qdot and transferred at the TIRF microscope. The position of 4–5 fields displaying labeled cells was saved at the automatized stage. Then, 125 ng/ml NGF was added to the medium and the cells of the selected fields were followed in a time course of eight points (0, 5, 10, 15, 30, 40, 50 and 60 min). For each cell and time point, we quantified the number of receptor spots per area. For comparing the internalization time-course of different cells, we normalized the spot density of each cell to its value at time 0. Cells with similar expression levels were chosen, excluding those with a number of moving receptors below 3.

Cell surface labeling of TrkA by Qdots and immunofluorescence in DRG neurons

Forty-eight hours after the transduction, DRG neurons were starved at 37°C for 1 h, then the membrane pool of receptors was biotinylated in two steps: (i) 30 min at 37°C with 10 μM Coenzyme A-biotin, 10 mM $MgCl_2$ and 2 μM Sfp synthase resuspended in cell medium and (ii) 60 min at 4°C with the same mix. Cells were washed two times with Hanks' Balanced Salt solution (HBSS, Sigma Aldrich-55021C) and incubated with 125-ng/ml NGF at 37°C for 60 min or were maintained in basal medium condition. After three washes with HBSS, cells were labeled at 4° for 15 min with 10 nM of streptavidin-Qdot (Qdot® 655 streptavidin conjugate; Invitrogen) in borate buffer at pH 8.3, 0.5% BSA and 215 mM sucrose. Cells were washed five times with HBSS and then fixed at RT for 15 min in PBS with 2% paraformaldehyde (PFA) and 5% of sucrose. After four washes with HBSS, neurons were permeabilized at RT for 5 min with a solution of PBS supplemented with 2.5% BSA and 0.1% Triton-X100. Neurons were blocked at RT for 1 h with a solution of 5% BSA in PBS and incubated at RT for 2 h with anti-TrkA (Millipore, 06-574, dilution 10 μg/ml) in PBS and 2.5% BSA. After three washes with PBS, cells were incubated at RT for 1 h with anti-rabbit Alexa 488 antibody (Thermo Fisher, dilution 1:100). The coverslips were finally mounted using Fluoroshield mounting medium (Sigma-Aldrich). Qdot655 was imaged using the 488 nm laser line, FF01-655/15 Semrock emission filter and a penetration depth of 110 nm while Alexa-488 using the 488 nm laser line with a 482–510 excitation filter and a 525/20 Leica emission filter.

For the analysis of the TrkA membrane versus total pool, ImageJ software was used. In detail, the fluorescence value of the background was subtracted in both Qdot (surface TrkA) and Alexa647 (total TrkA) channels. Then, a mask was drawn around the cell and the fluorescence intensity of Qdot655 ($I_{Qdot655}$) and Alexa647 ($I_{Alexa647}$) was measured. The fraction of surface S6-TrkA was derived by calculating the $I_{Qdot655}/I_{Alexa647}$ ratio, assuming a constant contribution of endogenous wt TrkA to the $I_{Alexa647}$ value.

Ethics statement on mouse experiments

All experimental procedures were performed in accordance with the Ministry of Health guidelines (Legislative Decree n°26/2014) and European Union 128 (Directive n°2010/63/UE) laws on animal research. The experiments were carried out in accordance with the ARRIVE guidelines (Animal Research: Reporting *in vivo* Experiments) and the principles of the Basel Declaration, including the '3R' concept. Efforts were made to reduce the number and discomfort of animals throughout the study.

Generation of knock-in human TkrA$^{R649W/m}$ mice

The mouse *Nrk1* gene is located on chromosome 3 and extends over 16.9 kb containing 17 exons separated by 16 introns, ATG translation initiation codon located in exon 1, and the STOP codon located in exon 17, 5′-UTR and 3′-UTR are located at 20 and 171 bp, respectively.

To generate the human TrkA$^{R649W/m}$ mouse line, the starting point was the targeting vector AMB1-Tg-pA, containing the coding sequence of the human NTRK1 (TRKA), that was used to generate the humanized wild-type TrkA knock-in mouse line (AMB1-TrkA/170608). Both the targeting vector AMB1-Tg-pA and the wild-type TrkA knock-in mouse line (AMB1-TrkA/170608) were kindly provided by Glenmark Pharmaceuticals. This humanized TrkA^{WT} knock-in mouse line is based on the in-frame replacement of the exon 1 coding sequence, as well as part of intron 1, of the murine Ntrk1 gene by the complete coding sequence of the human ortholog *NTRK1* gene.

We performed a site-specific mutagenesis PCR to introduce the HSAN IV R649W mutation in the targeting vector AMB1-Tg-pA containing the coding sequence of the human NTRK1. The mutated AflII-FseI segment from the AMB-Tg-pA vector replaced the AflII-FseI DNA segment of the vector AMB1-HR containing the *TrkA* human cDNA, long and short homology regions and the positive selection neomycin gene flanked by *Lox*P sites. Both plasmids AMB1-Tg-pA and AMB1-HR were supplied by Glenmark Pharmaceuticals.

The final targeting vector AMB1-HR carrying the R649W mutation in the humanized TrkA, was linearized prior to electroporation, then transfected into R1p.15 cells (background SV129) and positive clones were selected using neomycin resistance. Then, positive clones were injected into blastocysts from C57BL/6 mice and chimeric animals were crossed with 'Cre-deleter' mice expressing the Cre recombinase under the cytomegalovirus (CMV) promoter (Jackson Laboratories), to remove the neomycin selection cassette.

Southern blot analysis and genotyping

Genomic DNA was extracted by means of phenol:chloroform: isoamyl alcohol from cell clones electroporated with TrkA^{R649W} targeting vector. DNAs were first incubated with StuI (for 5′ screening), then positive clones were confirmed by AflII digestion (for 3′ screening). Digestions were run on a 0.8% agarose gel O/N at 50 V. After a mild depurination and denaturation, gels were blotted on nitrocellulose, and filters incubated with 5′ or 3′ probes. The internal 5′ probe was located within the 5′ homology sequence of TrkA targeting vector and detected an 11.3 kb band in the wild-type allele and a 6.4 kb band in recombinant alleles. The external 3′ probe was located downstream the 3′ homology sequence of the TrkA targeting vector, and labeled a 6.4 kb band in the wild-type allele and a 10.9 kb band in recombinant alleles.

Mice were genotyped by PCR. The following PCR primers were used:

fw_human: 5′-CTTGCTTGGCACTGTCCTCTCATGC-3′.
rev_human: 5′-TGCACAGCTAACCACTCCTCCATGG-3′.
fw_mouse: 5′-TGAGTGTGTGTCGTTCGGG-3′.
rev_mouse: 5′-ATGGGCTTAGGAACTTGGGC-3′.
Band sizes are: wild-type 343 bp, mutant 442 bp (Fig. 3B).

Behavioral analyses

All behavioral experiments were performed on TrkA$^{R649W/m}$, TrkA$^{h/m}$, NGF$^{R100W/m}$ and NGF$^{h/m}$ mice at 2 months of age. Both male and female mice were included. All animals were kept under a 12 h/12 h light/dark cycle, with food and water *ad libitum*. The experimenter was always blind to the genotype of the mice.

Cold sensitivity test

Mice were habituated for 30 min on an elevated platform with mesh flooring. Acetone (50 μl; Sigma-Aldrich) was applied onto the plantar surface of the hindpaw using a Hamilton syringe and the responses were scored as a four-point score: 0 = no response; 1 = paw withdrawal; 2 = repeated flicking of paw; 3 = licking of the paw. The acetone application was repeated six times by alternating the paw with an interval of 5 min. The frequency of response (expressed as a percentage) and the mean of the type of response (score response) was evaluated.

Hot plate test

Heat nociception was tested by hot plate test. After a habituation period (30 min), mice were placed on a surface heated at 48°C and the response latency, expressed as flicking or licking of the hindpaw, was noted. In order to avoid injury to the mice, a cut-off of 20 s was fixed.

Capsaicin injection test

To test the response to chemical noxious stimulus, capsaicin (catalog #141000, Abcam) was injected into the hindpaw of mice. Capsaicin was dissolved in dimethylsulfoxide (DMSO) and then diluted in saline to obtain the final concentration equal to 9 μg/μl. A total amount of 10 μl was injected in the ventral surface of the hindpaw using a Hamilton syringe. After the injection, mice were observed for 15 min and the time spent in licking the injected paw was measured. Control mice were injected with 10 μl of 0.1% DMSO in saline.

Tape response assay

Mice were acclimated in a plastic cage for 30 min. Then, a 3-cm piece of adhesive tape was placed gently on the mouse's back. Mice were observed for 5 min and the total number of bouts in response to the tape was recorded. Biting or scratching or 'wet dog shake' motion was scored as a response (57).

Mechanical sensitivity

Mechanical sensitivity was measured using the Von Frey Dynamic Plantar Aesthesiometer (Ugo Basile, Italy), which generates a mechanical force linearly increasing with time. The cutoff force was set at 20 g. After habituation (30 min) on an elevated platform with mesh flooring, the plantar surface of the mice hindpaw was stimulated by a single non-flexible filament and the force intensity was scored.

Sweat assay

A slightly modified standard method of sweat assay was performed (104). Mice were anesthetized (Zolpidem/xylazine 80–10 mg/kg) and pilocarpine (catalog #P6503, Sigma) was injected subcutaneously into the plantar surface of the foot (50 μg in 5 μl 0.9% saline). The injected paw was painted with 3.5% iodine (catalog #207772, Sigma-Aldrich) in ethanol, followed by coating with 10% starch solution in costar oil (both from Sigma-Aldrich). Sweating induced by pilocarpine was revealed by black spots formations on the plantar surface of the paw. The number of dark spots was measured 2, 5 and 10 min later (62).

Spontaneous alternation Y-maze test

A polyvinylchloride (PVC) maze consisting of three identical arms (40 × 13 × 10 cm) that converged at an equal angle was employed.

Each mouse was placed in the center of the maze and allowed to explore the arms freely during an 8-min session and recorded by video (Noldus Ethovision XT). An entry was scored when the mouse was at least halfway through an arm of the maze. An alternation was scored when all three arms were entered in consecutive events. The percentage of spontaneous alternations (% SAP) was calculated according to the following formula: % SAP = number of alternations/total entries × 100.

Novel object recognition test

The test was performed in 3 days. On day 1, mice were allowed to explore the empty arena (60 × 60 × 30 cm) for 10 min (habituation phase). On day 2, mice were exposed to two identical objects for 10 min to evaluate the total exploration time. On day 3, mice were exposed to a familiar object (namely A) and a new novel object (namely B) for 7 min (memory phase). The time spent exploring each object was recorded every day. We calculated a preference index by dividing the amount of time spent exploring the novel object by the total time spent exploring both objects. Mettere come è stato calcolato il preference index.

Elevated plus maze

The elevated plus maze consisted of two closed arms and two open arms (each 30 × 5 cm) extending from a central platform at 90°. Mice were placed on the central platform and allowed to freely explore the maze. The times spent in the open arms, closed arms and center were measured.

Three-chamber social approach test

Social approach behavior in mice was tested in the three-chamber apparatus as in (69), with minor modifications. First, the test mouse was habituated to the apparatus for 10-min in the center chamber, and then for additional 10-min with access to all three chambers. Then, the first stranger mouse (namely S1) and a novel object were placed into the two wire cups located in the opposite chambers of the apparatus (sociability phase). The test mouse was free to explore all three chambers for 10 min. The location of the novel object and stranger mouse was alternated across subjects. The time spent with the stranger mouse or the novel object was recorded. After the sociability phase, to evaluate the preference for social novelty, the test mouse was exposed for 10-min to a second novel stranger mouse (namely S2), which was placed into the wire cup where the object was previously located.

Immunohistochemistry

TrkA$^{h/m}$ and TrkA$^{R649W/m}$ mice were transcardially perfused with 4% PFA in PBS (pH 7.4%) and brains were dissected and post-fixed in the same solution, then cryoprotected in 30% sucrose in PBS for 72 h. About 45 μm-thick coronal sections were obtained using a freezing sliding microtome (Leica) and were collected in PBS and then immediately processed for immunohistochemistry. In detail, brain sections were washed three times in TBS with 0.3% Triton X-100, then treated with 3.5% H_2O_2 in TBS to inactivate endogenous peroxidases. Brain sections were treated with 10% FBS-0.3% Triton X-100 in TBS blocking solution for 30 min at RT. Then, the primary antibody (goat anti-ChAT 1:500 #AB144P, Millipore) was diluted in the same blocking solution and incubated 4°C O/N. The following day, after washing in TBS, the biotinylated anti-goat secondary antibody (Vector Laboratories) was diluted in 10% FBS in TBS for 3 h at RT. Sections were incubated in Vectastain ABC HRP Kit (Vector Laboratories) in PBS for 1 h and subsequently incubated in 3,3′-diaminobenzidine HCl (DAB, Sigma-Aldrich) and the enzyme Glucose Oxidase Type VII (Sigma-Aldrich) in TBS solution. The reaction was stopped within 10 min. Lastly, stained sections were mounted on glass slides, coverslipped using DPX Medium and acquired with a Nikon Eclipse E600 optical microscope. ImageJ program was used to measure the density of immunoreactive cells. Whole mount staining was performed on internal organs dissected from P0.5 pups, O/N fixed in 4% 273 PFA, then dehydrated in methanol series, followed by O/N quenching of endogenous peroxidases in 12 274 80% methanol, 17% DMSO, 3% H_2O_2. After rehydration, samples were blocked in 4% BSA, 1% 275 Triton X-100 in PBS, and incubated with 1:200 anti-TH antibody diluted in the same blocking 276 solution for 72 h at 4°C. The signal was revealed by incubation with HRP-conjugated anti-rabbit 277 antibody (1:200 Santa Cruz sc-2004) diluted in blocking solution O/N at 4°C, followed by DAB 278 processing. Finally, samples were cleared using a 2:1 solution of benzyl benzoate and benzyl 279 alcohol (BABB). Samples were imaged using a 4× objective and optical 280 density of the signal was quantified with the experimenter blind to the animal's genotype.

Skin and DRG immunofluorescence

DRG and skin (hairy and glabrous) were dissected and fixed with 4% PFA for 2 h or O/N 4°C, respectively. Tissues were cryoprotected in 30% sucrose in PBS O/N at 4°C, then embedded in OCT medium (Leica). Both DRG and skin were sectioned at a thickness of 40 μm using a cryostat (Leica). Sections were then treated with cold 50% ethanol for 30 min, followed by 2% BSA-0.3% Triton-X in PBS blocking solution for 1 h at RT, and finally incubated with primary antibodies in blocking solution O/N at 4°C. Secondary antibodies were diluted in blocking solution and incubated for 2 h at RT. Sections were mounted using DAPI-Fluoroshield™ Medium (Sigma). All images were acquired at 40× with a Leica SP2 confocal microscope and analyzed with ImageJ-Fiji (NIH, MD, 312 USA).

The following primary antibodies were used: 1:300 mouse anti-TRPV1 (Neuromics), 1:50 mouse anti-TrkA (MNAC13, 5.4 μg/μl) (105), 1:200 mouse anti-CGRP (Immunostar), 1:100 isolectin GS-B4-biotin conjugate (Invitrogen), 1:300 guinea pig anti-PV (Synaptic Systems), 1:200 rabbit anti-TH (Millipore), 1:500 mouse anti-NF200 (Sigma), 1:200 rabbit anti-PGP9.5 (Dako-Agilent), 1:300 guinea pig anti-VAChT (Synaptic System). All Alexa-conjugated secondary antibodies were used at 1:1000 concentration.

Statistical analysis

Data were analyzed using SigmaPlot 13 (Systat Software). Data are plotted as mean ± SEM. Details on the specific statistical tests used are reported in figure legends.

Supplementary material

Supplementary material is available at *HMG* online.

Acknowledgements

Authors' Contributions

Conceived the study: A.C. and S.C. Generation of genetically engineered mouse model: G.T. and M.C. Behavioural studies: P.P. and G.T. with support from S.C. and M.M. Neuroanatomical analyses in mice: P.P. and G.T. with support from S.C. and M.M. Biochemical analysis in cells: G.T. and J.A. *In vitro* biochemical and biophysics analysis: R.M., S.C. and L.M. Graphical illustrations: A.T. and P.P. Directed the project and supervised data analysis: A.C. and S.C. Wrote the manuscript: P.P., G.T., A.T., S.C. and A.C.

References

1. McMahon, S.B. (1996) NGF as a mediator of inflammatory pain. *Phil. Trans. R. Soc. A*, **351**, 431–440.
2. Levi-Montalcini, R. (1952) Effects of mouse tumor transplantation on the nervous system. *Ann. N. Y. Acad. Sci.*, **55**, 330–344.
3. Huang, E.J. and Reichardt, L.F. (2001) Neurotrophins: roles in neuronal development and function. *Ann. Rev. Neurosci.*, **24**, 677–736.
4. Levi-Montalcini, R. (1987) Years later. *Ann. NY Ac. Sci*, **55**, 330–344.
5. Kaplan, D.R., Hempstead, B.L., Martin-Zanca, D., Chao, M.V. and Parada, L.F. (1991) The trk proto-oncogene product: a signal transducing receptor for nerve growth factor. *Science*, **252**, 554–558.
6. Klein, R., Jing, S.Q., Nanduri, V., O'Rourke, E. and Barbacid, M. (1991) The trk proto-oncogene encodes a receptor for nerve growth factor. *Cell*, **65**, 189–197.
7. Chao, M.V., Bothwell, M.A., Ross, A.H., Koprowski, H., Lanahan, A.A., Buck, C.R. and Sehgal, A. (1986) Gene transfer and molecular cloning of the human NGF receptor. *Science*, **232**, 518–521.
8. Chao, M.V. (2003) Neurotrophins and their receptors: a convergence point for many signalling pathways. *Nat. Rev. Neurosci.*, **4**, 299–309.
9. Radeke, M.J., Misko, T.P., Hsu, C., Herzenberg, L.A. and Shooter, E.M. (1987) Gene transfer and molecular cloning of the rat nerve growth factor receptor. *Nature*, **325**, 593–597.
10. Chao, M.Y., Rajagopal, R. and Lee, F.S. (2006) Neurotrophin signalling in health and disease. *Clin. Sci.*, **110**, 167–173.
11. Levi-Montalcini, R., Skaper, S.D., Dal Toso, R., Petrelli, L. and Leon, A. (1996) Nerve growth factor: from neurotrophin to neurokine. *Trends Neurosci.*, **19**, 514–520.
12. Rizzi, C., Tiberi, A., Giustizieri, M., Marrone, M.C., Gobbo, F., Carucci, N.M., Meli, G., Arisi, I., D'Onofrio, M., Marinelli, S., Capsoni, S. and Cattaneo, A. (2018) NGF steers microglia toward a neuroprotective phenotype. *Glia*, **66**, 1395–1416.
13. Testa, G., Mainardi, M., Vannini, E., Pancrazi, L., Cattaneo, A. and Costa, M. (2022) Disentangling the signaling complexity of nerve growth factor receptors by CRISPR/Cas9. *FASEB J.*, **6**, e22498.
14. Barker, P.A., Mantyh, P., Arendt-Nielsen, L., Viktrup, L. and Tive, L. (2020) Nerve growth factor signaling and its contribution to pain. *J. Pain Res.*, **13**, 1223–1241.
15. Denk, F., Bennett, D.L. and Mcmahon, S.B. (2017) Nerve growth factor and pain mechanisms. *Annu. Rev. Neurosci.*, **40**, 307–325.
16. Pezet, S. and McMahon, S.B. (2006) Neurotrophins: mediators and modulators of pain. *Ann. Rev. Neurosci.*, **29**, 507–538.
17. Dyck, P.J., Peroutka, S., Rask, C., Burton, E., Baker, M.K., Lehman, K.A., Gillen, D.A., Hokanson, J.L. and O'Brien, P.C. (1997) Intradermal recombinant human nerve growth factor induces pressure allodynia and lowered heat-pain threshold in humans. *Neurology*, **48**, 501–505.
18. Lewin, G.R., Ritter, A.M. and Mendell, L.M. (1993) Nerve growth factor-induced hyperalgesia in the neonatal and adult rat. *J. Neurosci.*, **13**, 2136–2148.
19. Petty, B.G., Cornblath, D.R., Adornato, B.T., Chaudhry, V., Flexner, C., Wachsman, M., Sinicropi, D., Burton, L.E. and Peroutka, S.J. (1994) The effect of systemically administered recombinant human nerve growth factor in healthy human subjects. *Ann. Neur.*, **36**, 244–246.
20. Hefti, F.F., Rosenthal, A., Walicke, P.A., Wyatt, S., Vergara, G., Shelton, D.L. and Davies, A.M. (2006) Novel class of pain drugs based on antagonism of NGF. *Trends Pharm. Sci*, **27**, 85–91.
21. Sevcik, M.A., Ghilardi, J.R., Peters, C.M., Lindsay, T.H., Halvorson, K.G., Jonas, B.M., Kubota, K., Kuskowski, M.A., Boustany, L., Shelton, D.L. and Mantyh, P.W. (2005) Anti-NGF therapy profoundly reduces bone cancer pain and the accompanying increase in markers of peripheral and central sensitization. *Pain*, **111**, 128–141.
22. Ugolini, G., Marinelli, S., Covaceuszach, S., Cattaneo, A. and Pavone, F. (2007) The function neutralizing anti-TrkA antibody MNAC13 reduces inflammatory and neuropathic pain. *PNAS*, **104**, 2985–2990.
23. Dietz, B.W., Nakamura, M.C., Bell, M.T. and Lane, N.E. (2021) Targeting nerve growth factor for pain management in osteoarthritis—clinical efficacy and safety. *Rheum. Dis. Clin. N. Am.*, **47**, 181–195.
24. Lane, N.E., Schnitzer, T.J., Birbara, C.A., Mokhtarani, M., Shelton, D.L., Smith, M.D. and Brown, M.T. (2010) Tanezumab for the treatment of pain from osteoarthritis of the knee. *New Engl. J. Med.*, **363**, 1521–1531.
25. Einarsdottir, E., Carlsson, A., Minde, J., Toolanen, G., Svensson, O., Solders, G., Holmgren, G., Holmberg, D. and Holmberg, M. (2004) A mutation in the nerve growth factor beta gene (NGFB) causes loss of pain perception. *Hum. Mol. Genet.*, **13**, 799–805.
26. Indo, Y. (2001) Molecular basis of congenital insensitivity to pain with anhidrosis (CIPA): mutations and polymorphisms in TRKA (NTRK1) gene encoding the receptor tyrosine kinase for nerve growth factor. *Hum. Mut.*, **18**, 462–471.
27. Mardy, S., Miura, Y., Endo, F., Matsuda, I. and Indo, Y. (2001) Congenital insensitivity to pain with anhidrosis (CIPA): effect of TRKA (NTRK1) missense mutations on autophosphorylation of the receptor tyrosine kinase for nerve growth factor. *Hum. Mol. Gen.*, **10**, 179–188.
28. Mardy, S., Miura, Y., Endo, F., Matsuda, I., Sztriha, L., Frossard, P., Moosa, A., Ismail, E.A.R., Macaya, A., Andria, G. *et al.* (1999) Congenital insensitivity to pain with Anhidrosis: novel mutations in the TRKA (NTRK1) gene encoding A high-affinity receptor for nerve growth factor. *Am. J. Hum. Gen.*, **64**, 1570–1579.
29. Miranda, C., Di Virgilio, M., Selleri, S., Zanotti, G., Pagliardini, S., Pierotti, M.A. and Greco, A. (2002) Novel pathogenic mechanisms of congenital insensitivity to pain with anhidrosis genetic disorder unveiled by functional analysis

of neurotrophic tyrosine receptor kinase type 1/nerve growth factor receptor mutations. *J. Biol. Chem.*, **277**, 6455–6462.

30. Miranda, C., Zanotti, G., Pagliardini, S., Ponzetto, C., Pierotti, M.A. and Greco, A. (2002) Gain of function mutations of RTK conserved residues display differential effects on NTRK1 kinase activity. *Oncogene*, **21**, 8334–8339.

31. Capsoni, S. (2014) From genes to pain: nerve growth factor and hereditary sensory and autonomic neuropathy type V. *Eur. J. Neurosci.*, **39**, 392–400.

32. Indo, Y. (2018) NGF-dependent neurons and neurobiology of emotions and feelings: lessons from congenital insensitivity to pain with anhidrosis. *Neurosci. Biobeh. Rev.*, **87**, 1–16.

33. Minde, J., Toolanen, G., Andersson, T., Nennesmo, I., Remahl, I.N., Svensson, O. and Solders, G. (2004) Familial insensitivity to pain (HSAN V) and a mutation in the NGFB gene. A neurophysiological and pathological study. *Mus. Ner.*, **30**, 752–760.

34. Perini, I., Tavakoli, M., Marshall, A., Minde, J. and Morrison, I. (2016) Rare human nerve growth factor-β mutation reveals relationship between C-afferent density and acute pain evaluation. *J. Neuroph.*, **116**, 425–430.

35. Swanson, P.D. (1963) Congenital insensitivity to pain with anhidrosis. *Ann. Neur.*, **78**, 500.

36. Indo, Y., Tsuruta, M., Hayashida, Y. *et al.* (1996) Mutations in the TRKA/NGF receptor gene in patients with congenital insensitivity to pain with anhidrosis. *Nat. Genet.*, **13**, 485–488.

37. De Andrade, D.C., Baudic, S., Attal, N., Rodrigues, C.L., Caramelli, P., Lino, A.M.M., Marchiori, P.E., Okada, M., Scaff, M., Bouhassira, D. and Teixeira, M.J. (2008) Beyond neuropathy in hereditary sensory and autonomic neuropathy type V: cognitive evaluation. *Eur. J. Neur.*, **15**, 712–719.

38. Testa, G., Cattaneo, A. and Capsoni, S. (2021) Understanding pain perception through genetic painlessness diseases: the role of NGF and proNGF. *Pharm. Res.*, **169**, 105662.

39. Altassan, R., Saud, H.A., Masoodi, T.A., Dosssari, H.A., Khalifa, O., Al-Zaidan, H. and Wakil, S.M. (2017) Exome sequencing identifies novel NTRK1 mutations in patients with HSAN-IV phenotype. *Am. J. Med. Genet.*, **173**, 1009–1016.

40. Greco, A., Villa, R., Fusetti, L., Orlandi, R. and Pierotti, M.A. (2000) The Gly571Arg mutation, associated with the autonomic and sensory disorder congenital insensitivity to pain with anhidrosis, causes the inactivation of the NTRK1/nerve growth factor receptor. *J. Cell. Physiol.*, **182**, 127–133.

41. Moraes, B.C., Ribeiro-Filho, H.V., Roldão, A.P., Toniolo, E.F., Carretero, G.P.B., Sgro, G.G., Batista, F.A.H., Berardi, D.E., Oliveira, V.R.S., Tomasin, R., *et al.* (2022) Structural analysis of TrkA mutations in patients with congenital insensitivity to pain reveals PLCγ as an analgesic drug target. *Sci. Signal.*, **15**, eabm6046.

42. Chuang, H.H., Prescott, E.D., Kong, H., Shields, S., Jordt, S.E., Basbaum, A.I., Chao, M.V. and Julius, D. (2001) Bradykinin and nerve growth factor release the capsaicin receptor from PtdIns(4,5)P2-mediated inhibition. *Nature*, **411**, 957–962.

43. Verpoorten, N., Claeys, K.G., Deprez, L., Jacobs, A., Van Gerwen, V., Lagae, L. and Nelis, E. (2006) Novel frameshift and splice site mutations in the neurotrophic tyrosine kinase receptor type 1 gene (NTRK1) associated with hereditary sensory neuropathy type IV. *Neuromuscul. Disord.*, **16**, 19–25.

44. Shaikh, S.S., Chen, Y.C., Halsall, S.A., Nahorski, M.S., Omoto, K., Young, G.T., Phelan, A. and Woods, C.G. (2017) A Comprehensive Functional Analysis of NTRK1 Missense Mutations Causing Hereditary Sensory and Autonomic Neuropathy Type IV (HSAN IV). *Hum. Mutat.*, **38**, 55–63.

45. Arévalo, J.C., Waite, J., Rajagopal, R., Beyna, M., Chen, Z.Y., Lee, F.S. and Chao, M.V. (2006) Cell Survival through Trk Neurotrophin Receptors Is Differentially Regulated by Ubiquitination. *Neuron*, **50**, 549–559

46. Sánchez-Sánchez, J. and Arévalo, J.C. (2017) A review on ubiquitination of neurotrophin receptors: facts and perspectives. *Int. J. Mol. Sci.*, **18**, 630.

47. Kiris, E., Wang, T., Yanpallewar, S., Dorsey, S.G., Becker, J., Bavari, S., Palko, M.E., Coppola, V. and Tessarollo, L. (2014) TrkA in vivo function is negatively regulated by ubiquitination. *J. Neurosci.*, **34**, 4090–4098.

48. Yu, T., Calvo, L., Anta, B., López-Benito, S., López-Bellido, R., Vicente-García, C., Tessarollo, L., Rodriguez, R.E. and Arévalo, J.C. (2014) In vivo regulation of NGF-mediated functions by nedd4-2 ubiquitination of TrkA. *J. Neurosci.*, **34**, 6098–6106.

49. Amodeo, R., Nifosì, R., Giacomelli, C., Ravelli, C., La Rosa, L., Callegari, A., Trincavelli, M.L., Mitola, S., Luin, S. and Marchetti, L. (2020a) Molecular insight on the altered membrane trafficking of TrkA kinase dead mutants. *Biochim. Biophys. Acta Mol. Cell Res.*, **1867**, 8614.

50. Marchetti, L., Callegari, A., Luin, S., Signore, G., Viegi, A., Beltram, F. and Cattaneo, A. (2013) Ligand signature in the membrane dynamics of single TrkA receptor molecules. *J. Cell Sci.*, **126**, 4445–4456.

51. Amodeo, R., Convertino, D., Calvello, M., Ceccarelli, L., Bonsignore, F., Ravelli, C., Cattaneo, A., Martini, C., Luin, S., Mitola, S., Signore, G. and Marchetti, L. (2020b) Fluorolabeling of the PPTase-related chemical tags: comparative study of different membrane receptors and different fluorophores in the labeling reactions. *Front. in Mol. Bio.*, **7**, 1–10.

52. Callegari, A., Luin, S., Marchetti, L., Duci, A., Cattaneo, A. and Beltram, F. (2012) Single particle tracking of acyl carrier protein (ACP)-tagged TrkA receptors in PC12nnr5 cells. *J. Neurosci. Met.*, **204**, 82–86.

53. Chen, Z.-Y., Ieraci, A., Tanowitz, M. and Lee, F.S. (2005) A novel endocytic recycling signal distinguishes biological responses of Trk Neurotrophin receptors. *Mol. Bio. Cell*, **16**, 5761–5772.

54. Smeyne, R.J., Klein, R., Schnappt, A., Long, L.K., Bryant, S., Lewin, A., Lira, S.A. and Barbacid, M. (1994) Severe sensory and sympathetic neuropathies in mice carrying a disrupted Trk/NGF receptor gene. *Nature*, **368**, 17–20.

55. Haga, N., Kubota, M. and Miwa, Z. (2015) Hereditary sensory and autonomic neuropathy types IV and v in Japan. *Ped. Intern.*, **57**, 30–36.

56. Caterina, M.J., Schumacher, M.A., Tominaga, M., Rosen, T.A., Levine, J.D. and Julius, D. (1997) The capsaicin receptor: a heat-activated ion channel in the pain pathway. *Nature*, **389**, 816–824.

57. Ranade, S.S., Woo, S.H., Dubin, A.E., Moshourab, R.A., Wetzel, C., Petrus, M., Mathur, J., Bégay, V., Coste, B., Mainquist, J. *et al.* (2014) Piezo2 is the major transducer of mechanical forces for touch sensation in mice. *Nature*, **516**, 121–1250.

58. Li, L., Rutlin, M., Abraira, V.E., Cassidy, C., Kus, L., Gong, S., Jankowski, M.P., Luo, W., Heintz, N., Koerber, H.R., Woodbury, C.J. and Ginty, D.D. (2011) The functional organization of cutaneous low-threshold mechanosensory neurons. *Cell*, **147**, 1615–1627.

59. Peters, E.M.J., Hendrix, S., Gölz, G., Klapp, B.F., Arck, P.C. and Paus, R. (2006) Nerve growth factor and its precursor differentially regulate hair cycle progression in mice. *J. Histoc. Cytoc.*, **54**, 275–288.

60. Usoskin, D., Furlan, A., Islam, S., Abdo, H., Lönnerberg, P., Lou, D., Hjerling-Leffler, J., Haeggström, J., Kharchenko, O., Kharchenko, P.V., *et al.* (2015) Unbiased classification of sensory neuron types

by large-scale single-cell RNA sequencing. *Nat. Neurosci.*, **18**, 145–153.

61. Axelsson, H.E., Minde, J.K., Sonesson, A., Toolanen, G., Högestätt, E.D. and Zygmunt, P.M. (2009) Transient receptor potential vanilloid 1, vanilloid 2 and melastatin 8 immunoreactive nerve fibers in human skin from individuals with and without Norrbottnian congenital insensitivity to pain. *Neuroscience*, **162**, 1322–1332.

62. Liu, Y., Sebastian, B., Liu, B., Zhang, Y., Fissel, J.A., Pan, B., Polydefkis, M. and Farah, M.H. (2017) Sensory and autonomic function and structure in footpads of a diabetic mouse model. *Sci. Rep.*, **7**.

63. Testa, G., Calvello, M., Cattaneo, A. and Capsoni, S. (2019a) Cholinergic striatal neurons are increased in HSAN V homozygous mice despite reduced NGF bioavailability. *Bioch. Bioph. Res. Comm.*, **509**, 763–766.

64. Testa, G., Mainardi, M., Morelli, C., Olimpico, F., Pancrazi, L., Petrella, C., Severini, C., Florio, R., Malerba, F., Stefanov, A. *et al.* (2019b) The NGFR100W mutation specifically impairs nociception without affecting cognitive performance in a mouse model of hereditary sensory and autonomic neuropathy type V. *J. Neurosci.*, **39**, 9702–9715.

65. Levy Erez, D., Levy, J., Friger, M., Aharoni-Mayer, Y., Cohen-Iluz, M. and Goldstein, E. (2010) Assessment of cognitive and adaptive behaviour among individuals with congenital insensitivity to pain and anhidrosis. *Dev. Med. Child Neur.*, **52**, 559–562.

66. Kawade, H.M., Borkar, C.D., Shambharkar, A.S. and Singh, O. (2020) Pharmacology, biochemistry and behavior intracellular mechanisms and behavioral changes in mouse model of attention deficit hyperactivity disorder: importance of age-specific NMDA receptor blockade. *Pharm. Bioch. Behav.*, **188**, 172830.

67. Jeon, B.-J. and Son, S.-M. (2021) Social interaction changes in people with intellectual disabilities through the application of equine-assisted intervention in Korea. *Am. J. Transl. Res.*, **13**, 3573–3581.

68. Axelrod, F.B. and Gold-Von Simson, G. (2007) Hereditary sensory and autonomic neuropathies: types II, III, and IV. *Orph. J. Rare Dis.*, **2**, 39.

69. Chadman, K.K., Gong, S., Scattoni, M.L., Boltuck, S.E., Gandhy, S.U., Heintz, N. and Crawley, J.N. (2008) Minimal aberrant behavioral phenotypes of neuroligin-3 R451C knockin mice. *Autism Res.*, **1**, 147–141.

70. Yang, M., Silverman, J.L. and Crawley, J.N. (2011) Automated three-chambered social approach task for mice. *Curr. Prot. Neurosci.*, **8**, 26–33.

71. Basbaum, A.I., Bautista, D.M., Scherrer, G. and Julius, D. (2009) Cellular and molecular mechanisms of pain. *Cell*, **139**, 267–284.

72. Woolf, C.J. and Ma, Q. (2007) Nociceptors-noxious stimulus detectors. *Neuron*, **55**, 353–364.

73. Snider, W.D. and McMahon, S.B. (1998) Tackling pain at the source: new ideas about nociceptors. *Neuron*, **20**, 629–632.

74. Crowley, C., Spencer, S.D., Nishlmum, M.C., Chen, K.S., Pittsmeek, S., Armanlni, M.P., Llng, L.H., Mcmahon, S.B., Shelton, D.L., Levinson, A.D. and Phillips, H.S. (1994) Mice lacking nerve growth factor display perinatal loss of sensory and sympathetic neurons yet develop basal forebrain cholinergic neurons. *Cell*, **76**, 1001–1011.

75. Rosemberg, S., Marie, S.K.N. and Kiiemann, S. (1994) Congenital insensitivity to pain with anhidrosis (hereditary and autonomic Neur thy IV). *Ped. Neur.*, **11**, 50–56.

76. Liu, Z., Liu, J., Liu, G., Cao, W., Liu, S., Chen, Y., Zuo, Y., Chen, W., Chen, J., Zhang, Y. *et al.* (2018) Phenotypic heterogeneity of intellectual disability in patients with congenital insensitivity to pain with anhidrosis: a case report and literature review. *J. Int. Med. Res.*, **46**, 2445–2457.

77. Yu, T., Calvo, L., Anta, B., López-Benito, S., Southon, E., Chao, M.V., Tessarollo, L. and Arévalo, J.C. (2011) Regulation of Trafficking of Activated TrkA Is Critical for NGF-Mediated Functions. *Traffic*, **12**, 521–534.

78. Omerbašić, D., Smith, E.S.J., Moroni, M., Homfeld, J., Eigenbrod, O., Bennett, N.C., Reznick, J., Faulkes, C.G., Selbach, M. and Lewin, G.R. (2016) Hypofunctional TrkA accounts for the absence of pain sensitization in the African naked mole-rat. *Cell Rep.*, **17**, 748–758.

79. Babes, A., Zorzon, D. and Reid, G. (2004) Two populations of cold-sensitive neurons in rat dorsal root ganglia and their modulation by nerve growth factor. *Eur. J. Neurosci.*, **20**, 2276–2282.

80. Diogenes, A., Akopian, A.N. and Hargreaves, K.M. (2007) NGF Up-regulates TRPA1: implications for orofacial pain. *J. Dent. Res.*, **86**, 550–555.

81. Obata, K., Katsura, H., Mizushima, T., Yamanaka, H. and Kobayashi, K. (2005) TRPA1 induced in sensory neurons contributes to cold hyperalgesia after inflammation and nerve injury. *J. Clin. Inv.*, **115**, 2393–2401.

82. Story, G.M., Peier, A.M., Reeve, A.J., Eid, S.R., Mosbacher, J., Hricik, T.R., Earley, T.J., Hergarden, A.C., Andersson, D.A., Hwang, S.W. *et al.* (2003) ANKTM1, a TRP-like channel expressed in nociceptive neurons, is activated by cold temperatures. *Cell*, **112**, 819–829.

83. Davies, A.M., Bandtlowt, C., Heumannt, R., Korschingt, S., Rohrer, H. and Thoenen, H. (1987) Timing and site of nerve growth factor synthesis in developing skin in relation to innervation and expression of the receptor changes in NGF level. *Nature*, **326**, 353–358.

84. Ascaño, M., Richmond, A., Borden, P. and Kuruvilla, R. (2009) Axonal targeting of Trk receptors via transcytosis regulates sensitivity to neurotrophin responses. *Journal of Neuroscience*, **29**, 11674–11685.

85. Vaegter, C.B., Jansen, P., Fjorback, A.W., Glerup, S., Skeldal, S., Kjolby, M., Richner, M., Erdmann, B., Nyengaard, J.R., Tessarollo, L. *et al.* (2011) Sortilin associates with Trk receptors to enhance anterograde transport and neurotrophin signaling. *Nat. Neurosci.*, **1**, 54–63.

86. Zhang, K., Ben Kenan, R.F., Osakada, Y., Xu, W., Sinit, R.S., Chen, L., Zhao, X., Chen, J.Y., Cui, B. and Wu, C. (2013) Defective axonal transport of Rab7 GTPase results in dysregulated trophic signaling. *J. Neurosci.*, **33**, 7451–7462.

87. Tanaka, Y., Niwa, S., Dong, M., Farkhondeh, A., Wang, L., Zhou, R. and Hirokawa, N. (2016) The molecular motor KIF1A transports the TrkA neurotrophin receptor and is essential for sensory neuron survival and function. *Neuron*, **90**, 1215–1229.

88. George, L., Chaverra, M., Wolfe, L., Thorne, J., Close-Davis, M., Eibs, A. and Lefcort, F. (2013) Familial dysautonomia model reveals Ikbkap deletion causes apoptosis of Pax3+ progenitors and peripheral neurons. *PNAS*, **110**, 18698–18703.

89. Goffena, J., Lefcort, F., Zhang, Y., Lehrmann, E., Chaverra, M., Felig, J. and George, L. (2018) Elongator and codon bias regulate protein levels in mammalian peripheral neurons. *Nat. Commun.*, **9**, 889.

90. Jackson, M.Z., Gruner, K.A., Qin, C. and Tourtellotte, W.G. (2014) A neuron autonomous role for the familial dysautonomia gene ELP1 in sympathetic and sensory target tissue innervation. *Development*, **141**, 2452–2461.

91. Tourtellotte, W.G. (2016) Axon transport and neuropathy: relevant perspectives on the Etiopathogenesis of familial dysautonomia. *Am. J. Pathol.*, **186**, 489–499.

92. Minor, V. (1928) Ein neues Verfahren zu der klinischen Untersuchung der Schweißabsonderung. *Dtsch. Z. Nervenheilkd*, **101**, 301–308.

93. Itoh, Y; Yagishita, S. Nakajima, T. N. (1986). Congenital insensitivity to pain with anhidrosis: morphological and Morphometrical studies on the skin and peripheral nerves. *Neuropediatrics*, **17**, 103–110.

94. Pinsky, L. and DiGeorge, A.M. (1966) Congenital familial sensory neuropathy with anhidrosis. *J. Ped.*, **68**, 1–13.

95. Langer, J., Goebel, H.H. and Veit, S. (1981) Eccrine sweat glands are not innervated in hereditary sensory neuropathy type IV—an electron-microscopic study. *Acta Neuropathol.*, **54**, 199–202.

96. Nolano, M., Crisci, C., Santoro, L., Barbieri, F., Casale, R., Kennedy, W.R., Wendelschafer-Crabb, G., Provitera, V., Di Lorenzo, N. and Caruso, G. (2000) Absent innervation of skin and sweat glands in congenital insensitivity to pain with anhidrosis. *Clin. Neurophysiol.*, **111**, 1596–1601.

97. Morrison, S.F. (2016) Central neural control of thermoregulation and brown adipose tissue. *Auton. Neur.*, **196**, 14–24.

98. Ghasemlou, N., Krol, K.M., Macdonald, D.R. and Kawaja, M.D. (2004) Comparison of target innervation by sympathetic axons in adult wild type and heterozygous mice for nerve growth factor or its receptor trkA. *J. Pineal Res.*, **37**, 230–240.

99. Enomoto, H., Crawford, P.A., Gorodinsky, A., Heuckeroth, R.O., Johnson, E.M., Jr. and Milbrandt, J. (2001) RET signaling is essential for migration, axonal growth and axon guidance of developing sympathetic neurons. *Development*, **128**, 3963–3974.

100. Ernsberger, U. (2008) The role of GDNF family ligand signalling in the differentiation of sympathetic and dorsal root ganglion neurons. *Cell Tissue Res.*, **333**, 353–371.

101. Lefcort, F. (2020) Development of the autonomic nervous system: clinical implications. *Semin. Neurol.*, **40**, 473–484.

102. Marchetti, L., De Nadai, T., Bonsignore, F., Calvello, M., Signore, G., Viegi, A., Beltram, F., Luin, S. and Cattaneo, A. (2014) Site-specific labeling of neurotrophins and their receptors via short and versatile peptide tags. *PLoS One*, **9**, 1–18.

103. Gobbo, F., Bonsignore, F., Amodeo, R., Cattaneo, A., and Marchetti, L. (2018) Site-specific direct labeling of neurotrophins and their receptor: from biochemistry to advanced imaging applications. *Meth. Mol. Biol.*, **1727**, 295–314.

104. Tafari, A.T., Thomas, S.A. and Palmiter, R.D. (1997) Norepinephrine facilitates the development of the murine sweat response but is not essential. *J. Neurosci.*, **17**, 4275–4281.

105. Cattaneo, A., Capsoni, S., Margotti, E., Righi, M., Kontsekova, E., Pavlik, P., Filipcik, P. and Novak, M. (1999) Functional blockade of tyrosine kinase A in the rat basal forebrain by a novel antagonistic anti-receptor monoclonal antibody. *J. Neurosci.*, **19**, 9687–9697.